



UNIVERSIDADE FEDERAL DE SANTA CATARINA (UFSC)

CENTRO TECNOLÓGICO (CTC)

PROGRAMA DE PÓS-GRADUAÇÃO EM ENGENHARIA QUÍMICA

Angelo Oliveira Silva

Porous chitosan membranes with high porosity shaped by solvent evaporation technique in water as a solvent and acetone as a non-solvent

Florianópolis, Brasil

2022

Angelo Oliveira Silva

Porous chitosan membranes with high porosity shaped by solvent evaporation technique in water as a solvent and acetone as a non-solvent

Thesis presented to the Graduate Program in Chemical Engineering of the Federal University of Santa Catarina (UFSC) as a requirement for obtaining the Ph.D. title in Chemical Engineering.

Advisor: Prof. Dr. Ricardo Antonio
Francisco Machado

Co-advisors: Prof. Dr. Dachamir Hotza
Prof. Dra. Cintia Marangoni

Florianópolis, Brasil
2022

Ficha de identificação da obra elaborada pelo autor,
através do Programa de Geração Automática da Biblioteca Universitária da UFSC.

Silva, Angelo

POROUS CHITOSAN MEMBRANES WITH HIGH POROSITY SHAPED BY
SOLVENT EVAPORATION TECHNIQUE IN WATER AS A SOLVENT AND
ACETONE AS A NON-SOLVENT / Angelo Silva ; orientador,
Ricardo Machado, coorientador, Dachamir Hotza,
coorientador, Cintia Marangoni, 2022.

88 p.

Tese (doutorado) - Universidade Federal de Santa
Catarina, Centro Tecnológico, Programa de Pós-Graduação em
Engenharia Química, Florianópolis, 2022.

Inclui referências.

1. Engenharia Química. 2. Quitosana. 3. Membrana Porosa.
4. Destilação Por Membranas. I. Machado, Ricardo . II.
Hotza, Dachamir. III. Marangoni, Cintia IV. Universidade
Federal de Santa Catarina. Programa de Pós-Graduação em
Engenharia Química. V. Título.

Angelo Oliveira Silva

**POROUS CHITOSAN MEMBRANES WITH HIGH POROSITY SHAPED BY SOLVENT
EVAPORATION TECHNIQUE IN WATER AS A SOLVENT AND ACETONE AS A NON-
SOLVENT**

O presente trabalho em nível de Doutorado foi avaliado e aprovado por banca examinadora composta pelos seguintes membros:

Prof^a. Gabriela Carvalho Collazzo, Dr^a.
Universidade Federal de Santa Maria
Membro externo

Prof. Marco Di Luccio, Dr.
Universidade Federal de Santa Catarina
Membro externo

Emanoelle Diz Acosta, Dr^a.
Universidade Federal de Santa Catarina
Membro interno

Certificamos que esta é a **versão original e final** do trabalho de conclusão que foi julgado adequado para obtenção do título de doutor em Engenharia Química.

Prof^a. Débora de Oliveira, Dr^a.
Coordenadora do PósENQ

Prof. Ricardo Antonio Francisco Machado, Dr.
Orientador

*Dedico este trabalho a todos aqueles que
lutam pela qualidade da ciência e tecnologia
nacional*

ACKNOWLEDGMENTS

Firstly, I would like to thank God for the health, support, and wisdom conceived to me during my life journey.

To my advisor Professor Ricardo Machado, for being an amazing guide and leader for my research work during 10 years of cooperation.

To my co-advisors, Professor Dachamir Hotza, for all support, friendship, and consideration dedicated to my research work. Also, to Professor Cintia Marangoni for all the scientific contributions given in the field of membrane distillation, and also the permission to operate in the membrane distillation unit.

To my colleague and friends in LCP 4, in special to the biopolymers group: Ricardo Cunha, Karina Andrade, and Tailin Rieg, for friendship and partnership.

To my colleague and friends in LCP 3 linked to the membrane distillation unit, Regilene Sousa, Andressa Marafiga, for friendship and partnership.

To the LCME, Analysis Center, and LINDEN for being supported laboratory structure for the development of the present work.

To my other friends and family (Mother, Father, Aunts, Uncles, and Cousins) for the support and friendship all over these years.

To UFSC for the university infrastructure and opportunity to develop the research.

To CNPQ and CAPES for the funding values during this period.

“Nós nos transformamos naquilo que praticamos com frequência. A perfeição, portanto, não é um ato isolado. É um hábito” (Aristóteles)

ABSTRACT

Chitosan is one of the most common biopolymers and a promising candidate for membrane distillation. A porous hydrophobic membrane is required for this process, but synthetic polymers such as PVDF or PTFE are usually employed. In this work, a chitosan porous membrane was synthesized by solvent evaporation technique using acetone as a non-solvent. The membrane was characterized by wettability (contact angle, swelling index), open porosity, chemical (FTIR) and crystallographic properties (XRD), thermal analysis (DSC), and microstructure (N₂ adsorption, FEG-SEM). The best membranes were tested in the vapor permeation test. The solids and acetone concentrations strongly affect the membrane features. Water contact angle values presented a moderate hydrophobic behavior ($\Theta > 80^\circ$). Higher chitosan amounts linked to acetone tend to improve membrane hydrophobicity. According to the solution processing parameters, the open porosity values obtained are between 62% and 92%. Acetone promotes an increase in open porosity, swelling index, and a decrease in contact angle and crystallinity index. However, the conditions obtained are suitable for membrane distillation application. FTIR spectra show the formation of acetamido surface groups and changes in the degree of deacetylation. Acetone acts against surface functional groups of chitosan, and the decrease obtained in the degree of deacetylation may be associated with lower amino groups and, consequently, an increase in contact angle for membranes with 1 and 2 wt% of chitosan. DSC analysis indicates a shift in degradation temperature between the precursor powder and chitosan membranes. However, no significant changes in T_g were noticed. Membrane possesses slit-like pores in the meso and macroporous range. The membrane distillation tested with distilled water was successful and provided a high permeate flux ($16.07 - 51.62 \text{ kg} \cdot \text{m}^{-2} \cdot \text{h}^{-1}$), with an operating time of 2.5 h and a liquid entry pressure (LEP) of 1.1 bar, making the chitosan-based membranes good candidates to be tested in real effluent separation. Nevertheless, some improvements in processing conditions and membrane hydrophobicity could provide a higher LEP and a stabilization flux for an enhanced membrane distillation with chitosan material.

Keywords: Chitosan, Porous membrane, Acetone, Solvent evaporation, Membrane distillation.

RESUMO

A quitosana é um dos biopolímeros de uso mais comum e um candidato promissor para a destilação por membrana. Uma membrana hidrofóbica porosa é necessária para esse processo, no qual normalmente são empregados polímeros sintéticos como PVDF ou PTFE. Neste trabalho, uma membrana porosa de quitosana foi sintetizada por evaporação de solvente, usando acetona como antissolvente. A membrana foi caracterizada pela molhabilidade (ângulo de contato, índice de inchamento), porosidade aberta, propriedades químicas (FTIR) e cristalográficas (DRX), análise térmica (DSC) e microestrutura (adsorção de N₂, MEV-FEG). As melhores membranas obtidas foram testadas no teste de permeação de vapor por destilação. A concentração de sólidos totais e o teor de acetona empregado afetam fortemente as características da membrana. Os valores do ângulo de contato com a água indicam comportamento hidrofóbico moderado ($\Theta > 80^\circ$). Assim, maiores quantidades de quitosana ligadas à acetona tendem a aumentar a hidrofobicidade da membrana. Os valores de porosidade aberta obtidos estão entre 62 e 92%, de acordo com os parâmetros de processamento da solução. A concentração de acetona promove aumento da porosidade aberta, índice de inchamento, diminuição do ângulo de contato e índice de cristalinidade. Entretanto, as condições obtidas são adequadas para a aplicação de destilação por membrana. Os espectros de FTIR mostram a formação de grupos de superfície acetamido e mudanças no grau de desacetilação. Portanto, existe uma interação da acetona com os grupos funcionais de superfície da quitosana, e a diminuição obtida no grau de desacetilação pode estar associada à diminuição de grupos amino e, conseqüentemente, gerar um aumento no ângulo de contato das membranas com 1 e 2% de quitosana. A análise de DSC indica que há uma mudança na temperatura de degradação entre o pó precursor e as membranas de quitosana, porém, não há alterações significativas na Tg. A membrana possui poros em forma de fenda na faixa de meso e macroporosidade. A destilação por membrana testada com água destilada foi bem sucedida e forneceu um alto fluxo permeado ($16,07 - 51,62 \text{ kg} \cdot \text{m}^{-2} \cdot \text{h}^{-1}$), com um tempo de operação de 2,5 h e uma pressão de entrada de líquido (LEP) de 1,1 bar. Portanto, as membranas obtidas são boas candidatas para serem testadas em um efluente real, embora algumas melhorias nas condições de processamento e hidrofobicidade da membrana possam fornecer um LEP mais alto e um fluxo mais estável para uma destilação de membrana mais aprimorada com materiais à base de quitosana.

Palavras-chave: Quitosana, Membrana Porosa, Acetona, Evaporação de solvente; Destilação por membranas.

RESUMO EXPANDIDO

PRODUÇÃO DE MEMBRANAS POROSAS DE QUITOSANA COM POROSIDADE AUMENTADA PELA TÉCNICA DE COLAGEM POR SOLVENTE UTILIZANDO ACETONA COMO CO-SOLVENTE

Introdução

A Destilação por Membrana (DM) é aplicada para tratamento de efluentes e surge como uma alternativa mais econômica que os processos convencionais de destilação ou osmose reversa. DM é um processo termodinâmico de separação que utiliza o gradiente de pressão de vapor como força motriz para induzir uma transferência de calor e massa, por meio de uma membrana. A microestrutura e a hidrofobicidade da membrana atuam como uma barreira física que deve permitir apenas a transferência de vapor, criando uma interface líquido-vapor na entrada de cada poro da membrana, mantendo a passagem de líquidos, compostos não voláteis e sais dissolvidos.

Polímeros sintéticos como PVDF ou PTFE são normalmente empregados como membranas para DM e há uma carência de literatura sobre o uso de materiais de fonte renovável. Biopolímeros como a quitosana, com propriedades e microestrutura adequadas, são candidatos promissores para este tipo de aplicação.

A rota de conformação mais comum para membranas e filmes de quitosana é a colagem por solvente ou por solução. Esse método consiste em uma primeira dispersão do polímero sobre solventes ácidos orgânicos de baixa concentração, especialmente ácido acético, seguido por uma etapa de secagem para remoção completa do solvente. A técnica é limitada a uma estrutura específica de material, geralmente filmes finos depositados sobre uma superfície de vidro, e produz estrutura densa ou pouca porosa.

Em certas frações sólidas de quitosana, é possível adicionar quantidades de solventes orgânicos, como por exemplo a acetona, que pode produzir um ganho significativo de porosidade e área superficial por meio da técnica de evaporação de solvente. No entanto, é preciso avaliar o efeito da acetona na quitosana pura em diferentes concentrações, para a geração de poros em uma microestrutura de membrana e para aplicação em DM.

Objetivos

O objetivo deste trabalho é desenvolver membranas porosas de quitosana, pela rota de evaporação de solvente utilizando acetona como antissolvente, adequadas ao processo de destilação por membranas. Dentro desse escopo, está a avaliação da solubilidade da acetona no sistema de interação polímero/solventes, a influência no teor de sólidos ligado à quantidade de acetona nas propriedades físicas e químicas da membrana obtida. Além disso, deve-se investigar o desempenho da membrana de quitosana no processo de destilação por membrana, utilizando água destilada como fonte de alimentação.

Metodologia

Para a síntese das membranas utilizou-se, como material sólido precursor, a quitosana comercial em pó de média massa molar (Sigma-Aldrich, MM: 190.000-310.000, DD 75-85%), ácido acético glacial como aditivo, e acetona como co-solvente, bem como água deionizada que foi utilizada como solvente na produção das membranas.

Primeiramente, foram testadas amostras com diferentes teores de quitosana e razões de solventes (água e acetona). O preparo experimental consistiu em 4 etapas. A primeira etapa foi a preparação da solução diluída de ácido acético em água a uma concentração fixa de 1% em massa. A segunda etapa consistiu na mistura de todos os componentes; primeiramente, as quantidades de acetona definidas foram adicionadas e depois a quitosana foi acrescida ao sistema; nesta etapa, as amostras sem a adição de acetona foram testadas como controle. A terceira etapa corresponde à agitação do sistema na temperatura ambiente por 24 h até a solução ficar aparentemente homogênea; no entanto, pela parcial solubilidade da quitosana, persistiu sempre uma fração de insolúveis no corpo de fundo. A última etapa de secagem ocorreu na temperatura ambiente por 48 h, em capela com uma umidade relativa de ~60%. Para facilitar o processo de retirada da membrana seca, filmes de poliéster (Mylar) foram colados com fita adesiva dupla face sobre suportes de vidro, e testados para a produção da membrana (placas de Petri e lamínulas de vidro).

A molhabilidade da membrana foi mensurada, considerando suas alterações quanto ao teor de quitosana e de acetona, por meio de análise de ângulo de contato superficial aparente. O Grau de Inchamento de líquido (GI) pelos tipos diferentes de composição de membranas foi investigado. A determinação do grau de inchamento foi realizada pela diferença de massa de amostras pré-pesadas secas com a imersão em água destilada a temperatura ambiente e após a imersão por 48 h.

Analogamente ao grau de inchamento, a porosidade total pode ser estimada expandindo a expressão de cálculo. A fim de se avaliar qualitativamente o efeito da acetona na estrutura de membranas foi realizada Espectroscopia de Infravermelho por Transformada de Fourier, FTIR (Tensor 27, Bruker). O grau de desacetilação da quitosana também foi determinado por FTIR. Os difratogramas das membranas e o grau de cristalinidade (GC) foram obtidos por difração de raios X (DRX).

As medidas de calorimetria exploratória diferencial (DSC) foram realizadas para caracterizar as membranas e o pó precursor de quitosana, quanto à temperatura de degradação (T_d) e temperatura de transição vítrea (T_g). A análise porosimétrica foi realizada por adsorção e dessorção de N_2 e avaliação pelo método BJH. Finalmente, análises de microscopia eletrônica de varredura de alta resolução (MEV-FEG) da superfície das membranas foram realizadas para se verificar a morfologia dos poros obtidos.

A determinação da permeabilidade com água destilada com as membranas de quitosana no processo destilação por membranas por contato direto (DMCD) foi realizada com diferentes membranas e tempos de operação. Para finalizar as análises, a avaliação da pressão líquida de entrada (LEP) foi efetuada na melhor membrana obtida e seu valor comparado a valores comerciais.

Resultados e discussão

Pode-se perceber que existe um limite de solubilidade associado a uma razão volumétrica limite, de acordo com o aumento de acetona aplicada. Esse limite corresponde a um valor de 1:1 com 0,5% em massa de quitosana, 2:1 com 1,0% em massa de quitosana e 3:1 com 2,0% em massa de quitosana. Qualquer tentativa de incorporar uma maior quantidade de acetona na dispersão do sistema estudado gerou uma separação de fases muito intensa.

Conforme se aumenta a fração mássica de quitosana, maior será o ângulo de contato obtido e menor o grau de inchamento das membranas. Já em relação à de acetona, a absoluta maioria das membranas com acetona tendem a ângulos de contato maiores e grau de inchamento superiores do que as membranas sem acetona. Por fim, a razão volumétrica empregada promove um valor máximo de grau de inchamento e mínimo de ângulo de contato, sendo esse valor correspondente a uma diferença linear para o teor de sólidos de 3:1 para 0,5 %, de 5:1 para 1,0% e de 7:1 para 2,0% em massa de quitosana.

Os resultados mostraram uma variação de ângulo de contato de 83° a 112° , um comportamento moderadamente hidrofóbico e promissor ao processo de destilação por membranas. As membranas

tendem a ter pouco aumento ou alteração de hidrofobicidade, conforme o aumento de teor de sólidos nas amostras sem acetona, mas aliada a presença do outro solvente há maiores acréscimos dos ângulos de contato, conforme variações de razão volumétrica, principalmente nas amostras com 2% em massa de quitosana.

Os resultados de porosidade aberta apresentaram o mesmo comportamento dos resultados de grau de inchamento. Os valores obtidos estão na faixa de 62% a 92%, que são adequados ao processo de destilação por membranas. Condições empregadas de acetona produzem, em comparação com as membranas conformadas sem acetona, um ganho percentual de porosidade de 9,52% para amostras contendo 0,5%, 22,38% para as amostras contendo 1,0% e 16,12% para as amostras contendo 2,0% em massa de quitosana. Esses resultados demonstram a importância da presença na acetona na produção da microestrutura da membrana, e também da otimização da quantidade de acetona para um máximo ganho de porosidade e melhores resultados de fluxo posteriores.

Os espectros FTIR de todas as membranas avaliadas representam bem os picos característicos da quitosana e mostram também a dependência da concentração mássica de quitosana. O Grau de Desacetilação (GD) obtido a partir da curva de FTIR da amostra de quitosana em pó foi de 76,56 %, condizente ao que foi informado pelo fabricante (75-85%). Já o GD nas membranas não permaneceu constante. É possível perceber que existe uma tendência de queda do GD a um valor mínimo relativo nos pontos máximos de grau de inchamento e porosidade aberta para cada curva, especialmente os valores nas curvas de 1% e 2% em massa de quitosana que tendem a ter valores de GD bem inferiores à amostra de quitosana em pó de referência. Esses valores juntamente com os espectros FTIR podem indicar uma possível interação química dos grupamentos funcionais da quitosana precursora, que estariam se convertendo em radicais acetamino e, assim, ocorrendo uma reação de acetilação juntamente com a acetona produzindo da mesma forma grupos nitrila em certas condições.

É possível perceber, através dos espectros de DRX, as alterações cristalográficas da quitosana em pó para sua conformação em membranas, embora todas apresentem estruturas de um polímero semicristalino. Na amostra precursora em pó, pode-se notar uma região amorfa centralizado em $\sim 9^\circ$, que se desloca para $\sim 15^\circ$ nas conformações em membranas e aumenta também sua largura. Os índices de cristalinidade apresentados mostram uma leve diminuição entre a amostra em pó e as membranas, porém pouca alteração entre teor de sólidos e razão de água:acetona, permanecendo todos os valores entre 0,26-0,30.

Nos termogramas apresentados, é possível identificar na interseção das curvas a temperatura de transição vítrea (T_g por volta de 135°C) e a temperatura de início de degradação (T_d por volta de

240 °C) representada como a temperatura de começo do pico exotérmico, no qual ocorre a degradação das unidade de glucosamina. Conforme se aumenta o GD, diminui-se a Td, assim como esperado pela literatura. Já em relação à Tg, praticamente não há alteração em nenhuma das amostras testadas, nem na amostra em pó, nem nas membranas.

Isotermas de adsorção e dessorção de N₂ representam a distribuição de tamanho de poros na faixa de meso e macroporosidade. Nota-se, também, a presença de condensação capilar, representada pela aparição de um mesmo tipo de histerese em todas as amostras, sendo essa classificada como do Tipo H3, a qual caracteriza poros do tipo fenda, que é confirmado pela análise de MEV-FEG.

O desempenho das melhores membranas obtidas em DMCD rendeu elevados fluxos de permeado (16,07-51,62 kg·m⁻²·h⁻¹) porém com valores máximos de 2,5 h de operação. Variações de fluxo são correspondentes às diferentes propriedades físicas e químicas das membranas. Valores de LEP (1,1 bar) são adequados para o uso em destilação, porém podem ser aumentados por meio de uma modificação hidrofóbica para um fluxo mais estável e uma melhor aplicação.

Considerações finais

Os resultados obtidos mostraram que foi possível obter uma membrana biopolimérica de quitosana para o uso em destilação por membrana por uso da acetona como co-solvente na técnica de colagem por solvente. A solubilidade do sistema diminui com o aumento do teor de quitosana e de acetona. A rota de síntese realizada permitiu obter elevada porosidade, moderada hidrofobicidade e melhorado grau de inchamento. A acetona foi eficiente como agente porogênico, e possui um valor ótimo de concentração de acordo com o teor de quitosana empregado. Análises realizadas sugerem uma interação dos grupamentos funcionais da quitosana com a acetona, embora mais estudos sejam necessários para se concluir de fato o correto efeito de interação da acetona no meio de síntese. As membranas possuem poros na faixa de meso e macroporosidade, com poros do tipo fenda. A permeabilidade em destilação com água destilada foi possível. O fluxo de permeado obtido foi elevado e promissor para futuras aplicações, embora alterações na hidrofobicidade do material possam providenciar uma LEP maior e uma aplicação mais estável ao processo de destilação por membrana.

Palavras-chave: Quitosana, Membrana Porosa, Acetona, Colagem por solvente, Destilação por membranas.

LIST OF FIGURES

Figure 1- Structure of chitosan containing the amino, acetamido, and hydroxyl groups.	24
Figure 2- Schematic overview of the main stages of chitin and chitosan production.	25
Figure 3- Development history of chitin and chitosan scientific works.	27
Figure 4- Examples of covalent chemical reactions of functionalization on radicals: amino (NH ₂ , top) and hydroxyl (OH, bottom).	28
Figure 5- Examples of techniques for developing macroporous structures of chitosan according to their porosity and pore size.	31
Figure 6- Manufacturing process of porous structures derived from chitosan containing sacrificial material.....	31
Figure 7- Schematic representation of the membrane distillation process.	35
Figure 8- Conventional configurations of the membrane distillation process.	37
Figure 9- Evaluation criteria for membrane properties, membrane performance, and membrane distillation (MD) performance.	39
Figure 10- Process scheme of chitosan membrane (made with Biorender [®]).....	43
Figure 11- Petri dish and glass slips used in membrane drying steps.	44
Figure 12- Schematic of direct contact membrane distillation (DCMD) setup used to quantify the flux of water vapor transported across porous chitosan membranes.	48
Figure 13- Images of the membrane module applied.	49
Figure 14- Contact angle and swelling index for chitosan membrane according to water:acetone ratio and chitosan amount: (a) 0.5 wt% , (b) 1.0 wt%, and (c) 2.0 wt%.	51
Figure 15- Contact angle image for membrane containing 1 wt% chitosan with the increase of water:acetone solvent ratio.....	53
Figure 16- Open porosities of the chitosan membranes according to the water:acetone ratio and chitosan amount: (a) 0.5 wt%, (b) 1.0 wt% and (c) 2.0 wt%.	54
Figure 17- FTIR spectrum of the chitosan membranes and powder according to water:acetone ratio and chitosan amount: (a) 0.5 wt%, (b) 1.0 wt% and (c) 2.0 wt%	56
Figure 18- Degree of deacetylation from FTIR spectrum data for the chitosan membrane according to the water:acetone ratio and chitosan amount: (a) 0.5 wt%, (b) 1.0 wt% and (c) 2.0 wt%.	59
Figure 19- XRD spectra for the membrane containing 1 wt chitosan % with the increase of water:acetone volume ratio.	60

Figure 20- DSC thermograms of the powder and membranes containing 1 wt% chitosan with different water:acetone solvent ratio.....	62
Figure 21- Nitrogen adsorption-desorption isotherms for membranes with some selected water:acetone volume ratios and chitosan amounts.....	65
Figure 22- FEG-SEM pictures of the membranes with: (a) 1 wt% chitosan containing the following water/acetone ratio: A1 (1:0), A2 (5:1), (b) 2 wt% chitosan : B1 (1:0), B2 (7:1) (c) 0.5 wt% chitosan: C1(1:0), C2 (3:1), C3 (3:1) bottom view.....	66
Figure 23- Pure water permeate flux with 2 wt% chitosan in the membrane distillation unit during 1 h.....	68
Figure 24- Effect of the thickness (a), degree of deacetylation (b) and porosity (c) in relation to pure water permeate flux test for membrane 2 wt% chitosan in a membrane distillation unit for 1h.	70
Figure 25- Water permeate flux test on different times for membrane 2 wt% chitosan at 7:1 water/acetone volume ratio in the membrane distillation unit.....	71

LIST OF TABLES

Table 1- Separation process based on physical/chemical properties.	33
Table 2- Commercial values optimized for the membrane distillation process.....	40
Table 3- Overview of materials used.	43
Table 4- The main bands obtained in chitosan membranes FTIR.	57
Table 5- Crystallinity Index for some selected chitosan membranes.	61
Table 6- Glass transition temperature (Tg) and onset degradation temperature (Tonset) beginning of the chitosan powder and membranes containing 1 wt% with increasing acetone/water solvent ratio.....	63
Table 7- Comparison of experimental Liquid Entry Pressure (LEP) values in distilled water for PTFE, PP, PVDF commercial membranes and chitosan membrane obtained.	72

LIST OF ABBREVIATIONS

AGMD	Air Gap Membrane Distillation
BJH	Barret-Joyner-Halenda
CI	Crystallinity Index
DCMD	Direct Contact Membrane Distillation
DD	Degree of Deacetylation
DSC	Differential Scanning Calorimetry
FEG-SEM	Field Emission Gun- Scanning Electron Microscopy
FTIR	Fourier Transform Infrared
IUPAC	International Union of Pure and Applied Chemistry
LEP	Liquid Entry Pressure
MD	Membrane Distillation
PP	Poly(propene)
PTFE	Poly(1,1,2,2-tetrafluoroethylene)
PVDF	Poly-1,1-difluoroethene
SGMD	Stripping Gas Membrane Distillation
SI	Swelling Index
T _g	Glass transition temperature
T _{onset}	Degradation temperature
VMD	Vacuum Membrane Distillation
XRD	X-Ray Diffractometry

TABLE OF CONTENTS

1	INTRODUCTION.....	21
1.1	MOTIVATION	21
1.2	RESEARCH OBJECTIVES	22
1.3	THESIS STRUCTURE.....	23
2	LITERATURE REVIEW	24
2.1	CHITOSAN	24
2.1.1	Chitin and chitosan production	25
2.1.2	Conventional shaping processes and trends	27
2.1.3	Applications	29
2.1.4	Porosity generation	30
2.2	MEMBRANES	32
2.2.1	Membrane separation processes.....	32
2.2.2	Chitosan applied to membrane separation processes	33
2.3	MEMBRANE DISTILLATION	34
2.3.1	Configurations.....	36
2.3.2	Membranes properties and operational conditions	38
2.4	OVERVIEW	41
3	MATERIALS AND METHODS	42
3.1	MATERIALS.....	42
3.2	MEMBRANE SYNTHESIS	42
3.3	MEMBRANE CHARACTERIZATION	44
3.3.1	Contact angle, swelling index, and open porosity	44
3.3.2	Fourier-transform infrared spectroscopy (FTIR)	45
3.3.3	X-ray Diffractometry	46
3.3.4	Differential scanning calorimetry.....	46
3.3.5	Nitrogen adsorption and desorption porosimetry.....	46
3.3.6	Field emission gun scanning electron microscopy	47
3.4	MEMBRANE PERFORMANCE TESTS	47
4	RESULTS AND DISCUSSION	50
4.1	SYSTEM SOLUBILITY	50
4.2	MEMBRANE WETTABILITY AND POROSITY	50

4.3	CHEMICAL AND CRYSTALLOGRAPHIC PROPERTIES	55
4.4	THERMAL PROPERTIES.....	62
4.5	MEMBRANE MICROSTRUCTURE	64
4.6	PERFORMANCES OF MEMBRANES IN MD.....	68
4.7	OVERVIEW	73
5	CONCLUSIONS AND OUTLOOK.....	74
5.1	CONCLUSIONS.....	74
5.2	OUTLOOK	75
	APPENDIX A1- MEMBRANE CHARACTERIZATION	86
	APPENDIX A2- OVERVIEW OF THE MEMBRANE CHARACTERIZATION RESULTS	87

1 INTRODUCTION

1.1 MOTIVATION

Membrane Distillation (MD) is strongly applied for desalination or effluent treatment and emerges as an economical alternative to conventional distillation or reverse osmosis processes (EYKENS *et al.*, 2017; MADALOSSO *et al.*, 2020). MD is a thermodynamic process of separation that uses the gradient of vapor pressure as a driving force to induce heat and mass transfer matrix throughout the membrane (CAMACHO *et al.*, 2013; SILVA *et al.*, 2021b).

In this process, a volatile feed solution evaporates by slight heating, passes through submicron pores of a membrane, and condenses in the permeate solution at a lower temperature than the feed (GONZÁLEZ; AMIGO; SUÁREZ, 2017). The microstructure and hydrophobicity of the membrane act as a physical barrier that should only allow vapor transfer by creating a liquid-vapor interface at the entrance of each membrane pore while retaining the passage of liquid, non-volatile compounds, and dissolved salts (DUONG *et al.*, 2017; EYKENS *et al.*, 2016a; SILVA *et al.*, 2020). Thus, synthetic polymers such as PVDF or PTFE are usually employed (MADALOSSO *et al.*, 2021; SILVA *et al.*, 2021c), and there is a lack of literature about the use of renewable source materials for MD applications. Biopolymers such as chitosan, with proper shaping and microstructure properties, are promising candidates for this application.

Chitosan is defined as a semicrystalline copolymer of biological origin, derived from chitin and with cationic characteristics, consisting mainly of β -(1 \rightarrow 4)-2-acetamido-D-glucose and β -(1 \rightarrow 4)- 2-amino-D-glucose (SILVA *et al.*, 2021a). Chitin and Chitosan have a cellulose-like structure with a large presence of hydroxyls. However, instead of having a hydroxyl attached to the second carbon, they present an amino or acetamido group in its place, making these polymers of great commercial interest (BAKSHI *et al.*, 2020).

Chitosan materials have drawn growing attention as a promising renewable biopolymer soluble in aqueous acidic media (SAMPATH *et al.*, 2016; SILVA *et al.*, 2021a). The biggest advantages of biopolymers, such as chitosan, are non-toxicity, biocompatibility, and biodegradability. Also, different from the common synthetic polymers, the precursor raw materials come from renewable sources (GOOSEN, 1996). Therefore, chitosan has been increasingly used as a membrane precursor material for separation, concentration, and purifications in different membrane applications (VATANPOUR *et al.*, 2022).

Concerning membrane processes where the driving force of separation is temperature, chitosan and derivatives have been used in pervaporation (CASTRO-MUÑOZ; GONZÁLEZ-

VALDEZ; AHMAD, 2021; GRZYBEK *et al.*, 2022), in hydrophilic (CASTRO-MUÑOZ *et al.*, 2022), and oleophilic (SILVESTRE; BALDASSO; TESSARO, 2020) azeotropic separations. Despite these pervaporation applications, there is no deep investigation up to date on the use of chitosan as a membrane matrix in the MD process. The only works in this field have used chitosan as a coating on commercial PVDF membranes to lower the membrane fouling or improve properties in the membrane distillation process (AL-GHARABLI *et al.*, 2020; ARDESHIRI *et al.*, 2019).

The most common shaping route for chitosan membranes and films is denominated solvent or solution casting (BAKSHI *et al.*, 2020). This method consists of the first polymer dispersion in low concentrated organic acid solvents, especially acetic acid, following a drying step for complete solvent removal (MARTÍNEZ-CAMACHO *et al.*, 2010). The technique is limited to one specific material structure, to thin films usually deposited over a glass surface, and in the production of dense or low porous structure (ESMAEILI; RAJABI; BAKHTIARI, 2019).

When a slow and gradual drying step is applied in the solution casting method, it is possible to obtain a chitosan material with a submicrometric pore size (RUPIASIH *et al.*, 2017; RUPIASIH; SUMADIYASA; PUTRA, 2017). Based on this, Sahebamee *et al.* (2020) developed porous structures of chitosan and other hydrophilic polymers by applying acetone as a non-solvent together in the dissolution process. Knowing that in certain solid loadings of chitosan exist a certain tolerance to amounts of organic solvents with a small carbon chain (ROBERTS, 1992a), their results produced a significant gain in porosity and surface area in only one condition tested. However, their work did not evaluate the effect of pure chitosan on the presence of acetone at different concentrations and the optimized effect on the generation of pores in a membrane microstructure. Combining the chitosan membrane synthesis with the application in the membrane distillation process tends to improve the scientific knowledge of biopolymers in separation areas.

1.2 RESEARCH OBJECTIVES

This work has the general objective of developing a chitosan porous membrane synthesis by solvent evaporation technique using acetone as a non-solvent, producing a porous and hydrophobic material suitable for the membrane distillation process.

The specific objectives are:

- a) Evaluate a solubility study to state the maximum of acetone feasible to be incorporated in the process;

- b) Produce chitosan membrane with different solids amount and acetone/water volume ratios to understand the effect of solvent composition on the system;
- c) Investigate membrane properties obtained according to the membrane wettability, chemical, and crystallographic properties, thermal properties, and microstructure;
- d) Evaluate the membrane distillation viability by employing distilled water as a feed source and emphasizes the importance of developing an innovative source of raw material linked to the desired microstructure for a quality membrane distillation process.

1.3 THESIS STRUCTURE

This thesis is structured into five chapters. Chapters 1 and 2 comprise, respectively, the introduction and a literature review of relevant topics related to the present work. Research chapters are presented from Chapter 3 to Chapter 5.

Chapter 3 presents the materials and the equipment used. It also includes the description of the characterization methods of chitosan membrane and the conditions of membrane distillation tested. Chapter 4 introduces the results and discussion, comparing research works from the literature. Finally, in Chapter 5, the general conclusions and an outlook for future works are presented.

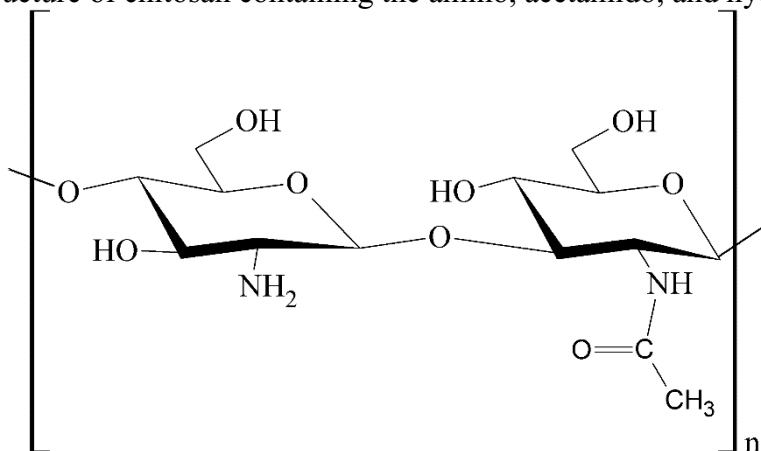
2 LITERATURE REVIEW

In this chapter, aspects related to the work available in the literature will be addressed. This literature review is divided into different parts to systematize the information, which is related to relevant works on chitosan, membranes, and membrane distillation process with its applications.¹

2.1 CHITOSAN

Chitosan is a biopolymer defined as a semicrystalline copolymer of biological origin, derived from chitin and with cationic characteristics, consisting mainly of β -(1 \rightarrow 4)-2-acetamido-D-glucose and β -(1 \rightarrow 4)- 2-amino-D-glucose (RODRIGUES, 2018; SILVA *et al.*, 2021a). Chitin and Chitosan have a cellulose-like structure with a high presence of surface hydroxyls radical, but instead of having a hydroxyl attached to the second carbon, they present an amino or acetamido group in this particular place, making these polymers of great commercial interest (BAKSHI *et al.*, 2020). Generally, the Degree of Deacetylation (DD) of chitosan, defined by the ratio of amino groups per acetamido, is between 40% and 98%, and the polymeric molar mass is between 50 and 2000 kDa (JAIN *et al.*, 2013). The chitosan structure is represented in Figure 1.

Figure 1- Structure of chitosan containing the amino, acetamido, and hydroxyl groups.



Ref: Author (2022).

Due to its biological and mechanical properties, chitosan has been widely used in the production of powders, hydrogels, membranes, fibers, and porous frameworks for biomedical applications, among others. This high adaptability of chitosan for a wide range of applications is

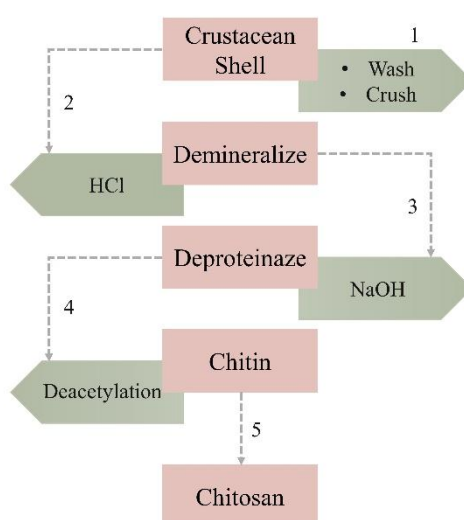
¹ Part of this Chapter was published as a review in Carbohydrate Polymers, Volume 272, 15 November 2021, 118472. <https://doi.org/10.1016/j.carbpol.2021.118472>

mainly due to a high degree of reactive amino functional groups present in D-glucosamine residues (SAMPATH *et al.*, 2016). These surface functional groups provide chitosan with several properties, including antimicrobial activity, chelating properties, high film-forming capacity, and high mechanical strength compared to other biopolymers (PRIYADARSHI; RHIM, 2020). The greatest advantage of biopolymers such as chitosan lies in their non-toxicity, biocompatibility, biodegradability, and their precursor raw material coming from renewable sources, thus diverging from synthetic polymers (GOOSEN, 1996).

2.1.1 Chitin and chitosan production

The biomass containing residues of crustacean exoskeletons, mainly shrimp, is the raw material precursor of chitin and chitosan. The chemical structure of crustacean shells is composed of protein, inorganic salts, chitin, and lipids (SILVA *et al.*, 2021a). The chitosan synthesis process comes from the chemical reaction of deacetylation of chitin from the initial biomass. The chemical deacetylation reaction and the global production overview are presented in Figure 2 (SILVA *et al.*, 2021a).

Figure 2- Schematic overview of the main stages of chitin and chitosan production.



Ref: Silva *et al.* (2021a).

Typically, the manufacturing process follows these unit operations (BAKSHI *et al.*, 2020; NASROLLAHZADEH *et al.*, 2021; RIAZ RAJOKA *et al.*, 2019):

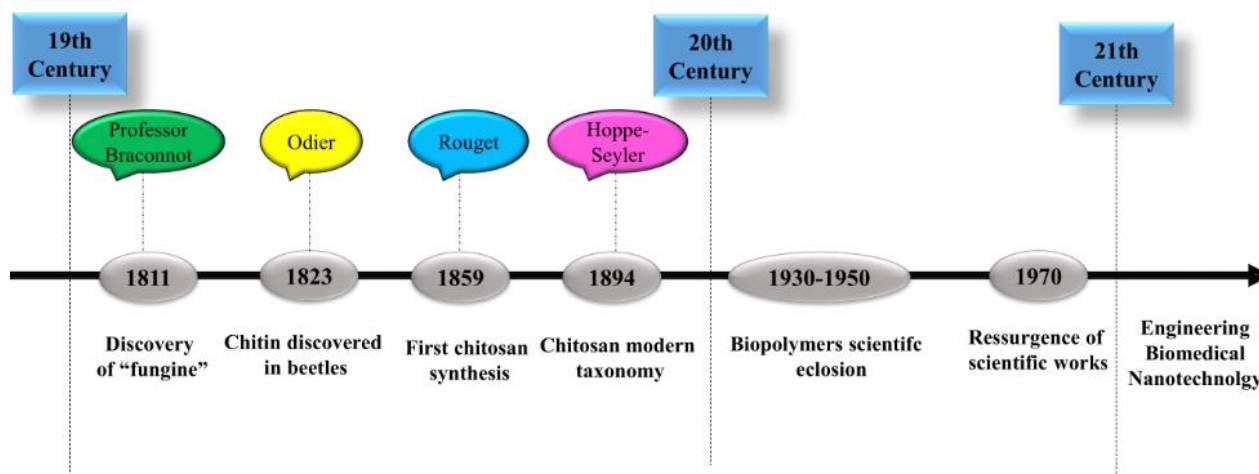
- i. The raw material shells are washed, crushed, and ground to smaller sizes with demineralization of some components, such as calcium carbonate, by chemical extraction with dilute hydrochloric acid with stirring at room temperature.
- ii. After demineralization, deproteinization is performed by applying dilute aqueous sodium hydroxide solution. Proteins can be recovered by lowering the pH to 4.0 and then drying the precipitates.
- iii. An additional decolorization step may be incorporated to remove color. In this step, chitin is extracted as the main input material to produce chitosan.
- iv. Chitosan is obtained by deacetylation from the chitin obtained, again in sodium hydroxide but in an environment without oxygen and sometimes by an enzymatic route. The three key reaction parameters are alkali concentration, time, and temperature. Those factors define the degree of deacetylation of the final material.

The history of chitin and chitosan production is relatively old and dates back to works developed in the 19th century (Figure 3). The first explicit description of the discovery of chitin was written in 1811 by Braconnot (BRACONNOT, 1811), who renamed the alkali-resistant fraction of isolates of some higher fungi or "fungine".

In 1823, the Odier found a material with the same general properties as "fungine" in the cuticle, or carapace, of beetles and named this material "chitin", which refers to the Greek word "chiton" which means "coating", referring to the tunics worn by the ancient Greeks and Romans. Rouget (ROUGET, 1859) promoted the boiling of chitin in potassium hydroxide and found that it became soluble in organic acids leading to the discovery of chitosan in 1859. In 1894, Hoppe-Seyler (HOPPE-SEYLER, 1894) renamed this material with the current taxonomy of chitosan.

The 1930s–1950s were when the production of numerous scientific articles published on the uses of chitin and chitosan began. In the following decades, after the Second World War, the invention of synthetic fibers appeared that obscured the study of these products and other biopolymers. Only from the 1970s onwards, there was a resurgence of interest in biopolymers, and studies on chitin and chitosan have increased since then (BAKSHI *et al.*, 2020). Many research works using chitosan as a source of potential bioactive material appeared in the last 40 years (RAMYA *et al.*, 2012).

Figure 3- Development history of chitin and chitosan scientific works.



Ref: Adapted from Bakshi *et al.* (2020).

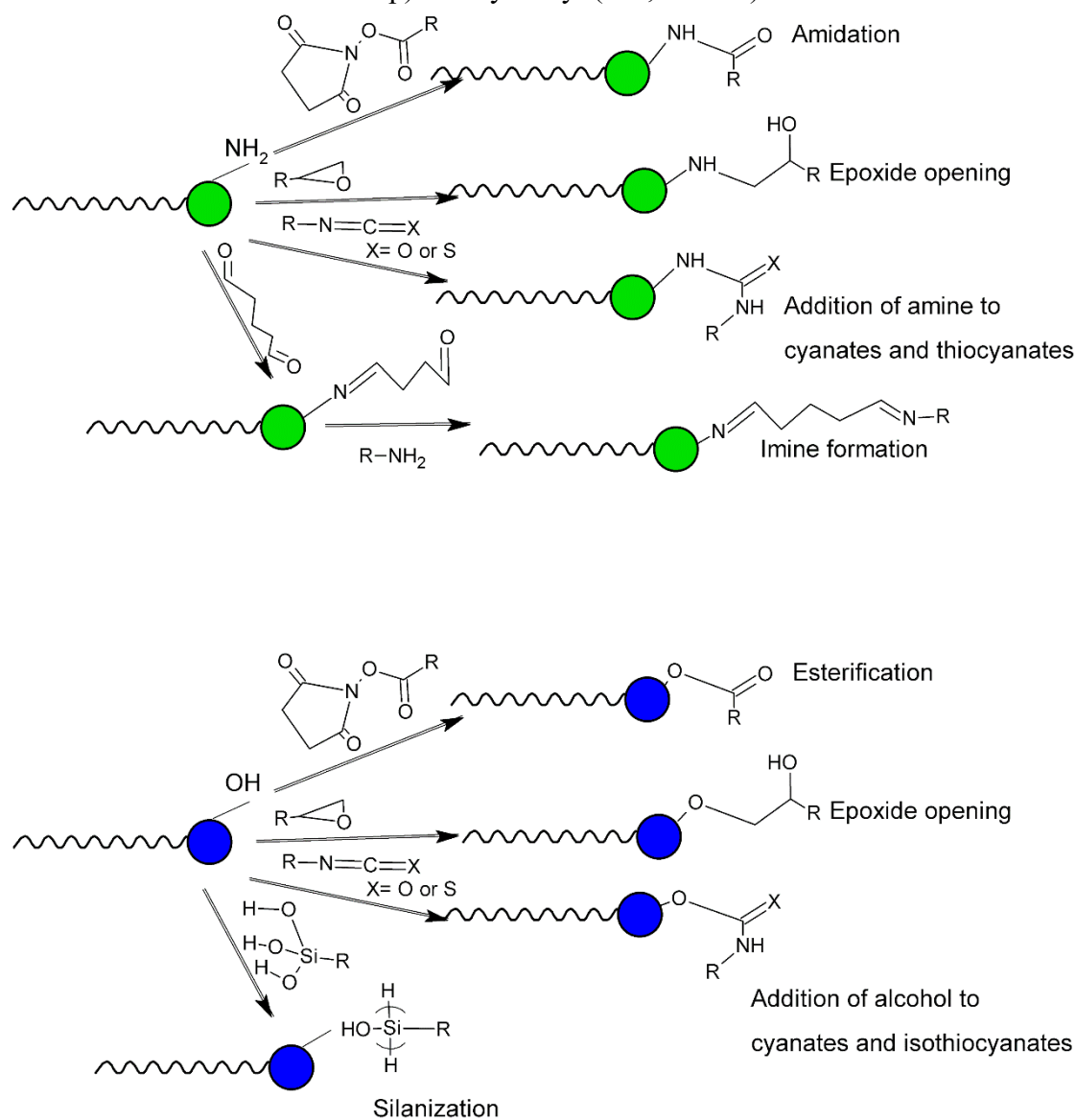
2.1.2 Conventional shaping processes and trends

The main route for chitosan shaping is known as solvent or solution casting (BAKSHI *et al.*, 2020). This method consists of dispersing the chitosan biopolymer in solvents based on organic acids, especially acetic acid, followed by a phase of complete solvent evaporation (MARTÍNEZ-CAMACHO *et al.*, 2010). This technique is limited to a specific material structure, in the case of films deposited on a glass surface, and in the production of dense or lower porous structures (ESMAEILI; RAJABI; BAKHTIARI, 2019). Sometimes additives are needed, such as glycerol, which acts as a plasticizing agent and provides an improvement in the characteristics of the film produced (CUI; BEACH; ANASTAS, 2011).

The physical and chemical characteristics of the films produced by solvent casting, such as thickness, contact angle, swelling index, crystallinity index, degradation temperature, permeability and mechanical properties, strongly depend on initial processing parameters, such as the organic acid that was chosen as the solvent and its pH (CHEN *et al.*, 2007; KIM *et al.*, 2006); the degree of deacetylation of the raw material and the molar mass (BASKAR; KUMAR, 2009); and the mass concentration of chitosan applied (RUPIASIH; SUMADIYASA; PUTRA, 2017).

As mentioned before, chitosan has significant amino and hydroxyl functional groups, which are strongly reactive to other organic/inorganic species and lead to the coupling of structures and production of derivative chitosan species, or still to immobilizing enzymes or adding nanoparticles. Examples of covalent chemical reactions in the amino and hydroxyl groups of chitosan are shown in Figure 4.

Figure 4- Examples of covalent chemical reactions of functionalization on radicals: amino (NH_2 , top) and hydroxyl (OH , bottom).



Ref: Silva *et al.* (2021).

Currently, chitosan and its derivatives have been processed in the most different types of possible production routes, with the emphasis on more elaborate and robust conformations, such as electrospinning and 3D printing (SILVA *et al.*, 2021a). However, there is a lot of research gap in the development of macro, meso, and microporous controlled structures of chitosan for an adequate application in membranes, which will be discussed in more detail in item 2.1.4.

2.1.3 Applications

According to literature, chitosan has a wide range of applications in areas of great technological impact, such as pharmacology, agriculture, and industry, among others (ZHU; ARSOVSKA; KOZOVSKA, 2017). Research work related to chitosan and its derivatives has focused heavily on the areas of wastewater treatment, tissue engineering, and protective coatings (SILVA *et al.*, 2021a).

Chitosan as a filter/membrane matrix for water and wastewater treatment has gained significant interest in recent years (PAKDEL; PEIGHAMBARDOUST, 2018; THIRUGNANASAMBANDHAM; SIVAKUMAR; MARAN, 2013). Crini *et al.* (2017) described the use of chitosan in the ultrafiltration (UF) process, where a wide variety of metal ions can be adsorbed and selectively separated. Chitosan-derived metallic nanocomposites emerge as a potential material to promote efficient and sustainable dye removal (RASHID *et al.*, 2018). The high adsorption capacity of heavy metals by chitosan and its derivatives is related to its functional groups, hydrophilicity, high chemical reactivity, and flexible polymeric structure (VUNAIN; MISHRA; MAMBA, 2016). The amino and hydroxyl groups of chitosan can produce stable chelates in contact with transition metal ions, such as Hg^{2+} , Ni^{2+} , Cu^{2+} , Pb^{2+} , Zn^{2+} , Cd^{2+} (GUPTA; KUSHWAHA; CHATTOPADHYAYA, 2012) making chitosan act as a bioadsorbent. This ability to remove contaminants from chitosan is mainly related to the surface area of the chitosan membrane and its conformation (ZHU *et al.*, 2021).

Chitosan has also been extensively studied in biomedical fields, such as the production of cellular scaffolds, wound healing, drug administration, dietary supplements, and biosensors, among others. Consequently, chitosan has already been applied to help solve various human health condition problems: blood clotting, healing of skin burns, control of food allergies and intolerance, weight loss and cholesterol control, gene therapy, and cancer treatment, among others (RIZEQ *et al.*, 2019). Chitosan in pharmaceutical tablets is commonly seen within dietary supplements for fat burning and malignant cholesterol reduction and can reduce weight gain by electrostatically attaching fatty acids released by digestion in the small intestine (SHARIATINIA, 2019).

Finally, one of the most common ways chitosan materials are used is in protective coatings. Especially on metallic substrates, chitosan is a polysaccharide with strong anti-corrosion potential and easy adhesion (QASIM *et al.*, 2019; UMOREN; EDUOK, 2016). Due to this coating and protection potential, chitosan and its derivatives have also been used in the production of food packaging (WU *et al.*, 2019).

2.1.4 Porosity generation

In relation to the total porosity of solids, they can be dense structures or without porosity, or porous, i.e., those containing a certain amount of voids. According to International Union of Pure and Applied Chemistry (IUPAC), considering the pore size for a given type of material, macro (>50 nm), meso (2-50 nm), or micropores (<2 nm) can be defined (SAMPATH *et al.*, 2016).

In the development of chitosan-derived materials, a great challenge persists in developing structures with pores below 1 μm linked to high open porosity. For the most part, it produces very large pores or dense structures (SAMPATH *et al.*, 2016; SILVA *et al.*, 2021a).

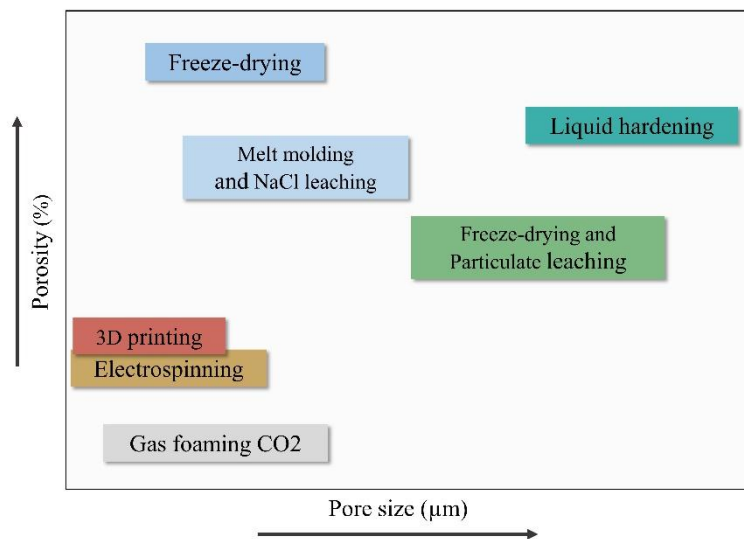
For the generation of macroporosity, alternative processes have been applied, such as lyophilization (SULTANA *et al.*, 2015), electrospinning (MURALI *et al.*, 2020), 3D printing (SAHRANAVARD *et al.*, 2020), and traditional procedures using some sacrificial material, such as particulates or solvents (DELGADO-RANGEL *et al.*, 2020; SILVA *et al.*, 2021a). The production of chitosan macroporous structures is exemplified in Figure 5.

The production processes of macroporous chitosan membranes containing sacrificial material have already been widely applied in the literature, mainly with the use of silica as a porogenic agent and treatment with NaOH as a removal agent (XU; HEIN; WANG, 2008; ZENG; RUCKENSTEIN, 1996). In this way, symmetrical and asymmetrical structures of chitosan and chitin have been produced, as illustrated in Figure 6.

Usually, when the production is carried out using solvent casting with a slow and gradual drying step, a material with submicrometric pores is obtained (RUPIASIH *et al.*, 2017; RUPIASIH; SUMADIYASA; PUTRA, 2017). This opens many applications in membrane separation processes, but still, these materials persist with low porosity and little applicability in an industrial view (SEDELKIN *et al.*, 2019). The development of porous chitosan structures can also be obtained by the dissolution technique in the presence of a non-solvent or cosolvent by solvent evaporation technique (BEPPU; ARRUDA; SANTANA, 1999; HONG; WEI; LIU, 2007). In this way, Sahebamee *et al.* (2020) developed porous structures of chitosan and other hydrophilic polymers by applying acetone as a non-solvent together in the dissolution process. In certain mass amounts of chitosan, there is a certain tolerance to amounts of organic solvents with a small carbon chain. Experimental results (ROBERTS, 1992b) showed a significant gain in porosity and surface area in only one condition tested. However, this work lacked to evaluate the effect of pure chitosan on the presence of acetone

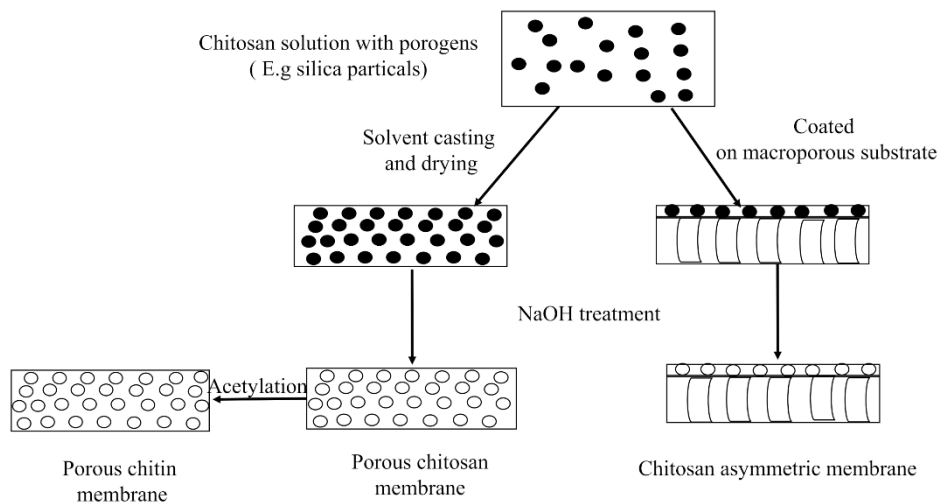
at different concentrations and in this way, reach an optimized effect on the generation of pores in a membrane microstructure.

Figure 5- Examples of techniques for developing macroporous structures of chitosan according to their porosity and pore size.



Ref: Silva *et al.* (2021).

Figure 6- Manufacturing process of porous structures derived from chitosan containing sacrificial material.



Ref: Adapted from Xu, Hen and Wang (2006).

2.2 MEMBRANES

A membrane can be defined as a selective barrier between two phases, where the term “selective” is inherent to a membrane or a membrane separation process (MULDER, 1996). Generally, a membrane is a barrier that separates or restricts partly or totally the passage of a specific chemical species due to its characteristics. This membrane can be homogenous or heterogeneous, present positive, negative, or neutral charge, or even be bipolar, symmetric, or asymmetric. Moreover, it can be active or passive, and driven by pressure, concentration, or temperature difference. The membranes also can be porous or dense and composed of various materials. In addition, the separation drive force can be obtained by pressure, concentration, or temperature gradient (BIRON; SANTOS; ZENI, 2018).

The material from which the membrane is made will depend on the requirements imposed and the kind of process used. The species taken from the membrane can be called retentate or concentrated matter, while the species which cross the membrane structure are denominated permeate or filtered matter.

The most common industrial processes involving separation membranes are microfiltration, ultrafiltration, nanofiltration, and reverse osmosis (ALZHRANI; MOHAMMAD, 2014), which use pressure gradient as a driven force. In those cases, the selectivity and filtration capacity, as well as the quality of the permeate flux are mainly defined by the pore size of the membrane and open porosity (PEARCE, 2007).

2.2.1 Membrane separation processes

The membrane separation processes are very attractive and promising for several technological fields, such as water and wastewater treatment, biotechnology, food, and beverages production, among others (BIRON; SANTOS; ZENI, 2018; PENDERGAST; HOEK, 2011; RAMLOW; MACHADO; MARANGONI, 2017; ZHANG; ZHONG; XING, 2013).

The membrane separation processes are defined by gradients of pressure, concentration, or electric field across the membrane and can be differentiated according to the type of driving force, molecular size, or type of operations (LI, 2007). A classification of some membrane separation processes in terms of physical or chemical properties of the components to be separated is given in Table 1.

Table 1- Separation process based on physical/chemical properties.

Physical/ chemical property	Separation process
Size	Filtration, microfiltration, ultrafiltration, nanofiltration, dialysis, gas separation, gel permeation chromatography
Vapor Pressure	Membrane distillation, pervaporation
Freezing Point	Crystallization
Affinity	Extraction, adsorption, absorption, reverse osmosis.
Charge	Ion exchange, electrodialysis, electrophoresis, diffusion dialysis
Density	Centrifugation
Chemical Nature	Complexation, carrier-mediated transport

Ref: Adapted of Mulder (1996).

2.2.2 Chitosan applied to membrane separation processes

Chitosan has been extensively tested along with other materials, in various types of configurations and membrane separation processes (XU; HEIN; WANG, 2008). Besides to the aforementioned application in item 2.1.3 of chitosan as ion adsorption membranes, and the possibility exemplified in item 2.1.4 (SEDELKIN *et al.*, 2019) in micro, ultra, and nanofiltration. There is plenty of other membrane separation process able to be applied with chitosan derivative materials.

Yang e Zall (1984) realized the potential use of chitosan in the reverse osmosis process and concluded that, in some ways, chitosan works better than cellulose acetate because of its greater resistance at a high alkaline concentration, in addition to the durability in the presence of some organic solvents. The use of chitosan in membranes for gas separation, mainly related to CO₂ capture, has increased in recent decades (BORGOHAIN *et al.*, 2021; ZARGAR; ASGHARI; AFSARI, 2019). The moderately hydrophilic nature of chitosan is feasible to obtain a better CO₂ separation from gases such as N₂, H₂, among others.

The amino and hydroxyl functional groups of a chitosan membrane allow the complexation of metals along with the ultrafiltration process (KAMIŃSKI; MODRZEJEWSKA, 1997). Furthermore, due to the easy film production, Wu *et al.* (2011) developed a membrane with an inert matrix of chitosan, which allows a process of crystallization of inorganic salts, such as CaCO₃.

The conditions of biodegradability and biocompatibility also allow the use of chitosan in dialysis and hemodialysis membranes (AYUNI; YUNINGRAT, 2017; RADHAKUMARY *et al.*,

2006). Chuang, Chen e Chen (2014) produced a mesoporous membrane of chitosan for microdialysis using gelatin nanoparticles as the sacrificial material; the authors had a maximum limit of obtaining an open porosity of 38% pores in the range from 40 to 100 nm, as a function of the chitosan radius and applied gelatin. Membrane properties show no cytotoxic signal for *in vitro* systems.

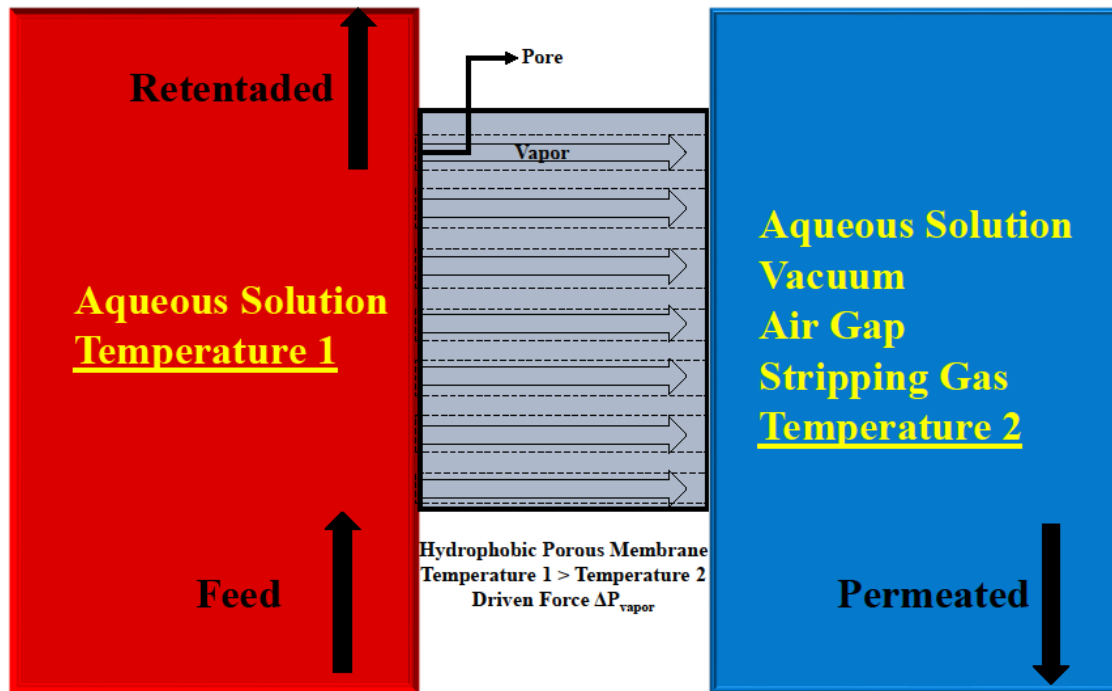
In processes where the driving force of separation is temperature, chitosan and its derivatives have been strongly used in pervaporation (CASTRO-MUÑOZ; GONZÁLEZ-VALDEZ; AHMAD, 2021), whether in asymmetric structures (GRZYBEK *et al.*, 2022), or hydrophilic azeotropic (CASTRO-MUÑOZ *et al.*, 2022) and oleophilic separations (SILVESTRE; BALDASSO; TESSARO, 2020). Despite all these applications in pervaporation, no work is available to date on the use of chitosan as a membrane matrix in Membrane Distillation (MD). The only works found are related to the use of chitosan as a coating on commercial PVDF membranes to lower the membrane fouling or improve the membrane distillation process (AL-GHARABLI *et al.*, 2020; ARDESHIRI *et al.*, 2019).

2.3 MEMBRANE DISTILLATION

Membrane Distillation (MD) emerges as an alternative with lower energy costs than conventional distillation or reverse osmosis processes (SANTOS, 2021). MD is a thermodynamic process of separation that uses heat and mass transfer force through the gradient of the vapor pressure difference between the membrane as matrix force (CAMACHO *et al.*, 2013). The temperature gradient on the outer surfaces of the membrane induces this vapor pressure difference on both sides, resulting in a flux of heat and mass through the microstructure, as exemplified in Figure 7.

In the MD process, a volatile feed solution evaporates by slight heating, passes through submicron pores of a membrane, and condenses in the permeate solution, which is at a lower temperature than the feed (GONZÁLEZ; AMIGO; SUÁREZ, 2017). The microstructure and hydrophobicity of the membrane act as a physical barrier that should only allow vapor transfer by creating a liquid-vapor interface at the entrance of each membrane pore while retaining the passage of liquid, non-volatile compounds, and dissolved salts (DUONG *et al.*, 2017; EYKENS *et al.*, 2016b). The mass transfer is initiated by the evaporation of the feed liquid at the liquid-vapor phase boundary in the pores and the vapor pressure gradient induces the diffusion of vapor molecules across the membrane (SANTOS, 2021). Condensation of the vapor takes place later on the permeate side (EYKENS *et al.*, 2016b).

Figure 7- Schematic representation of the membrane distillation process.



Ref: Adapted from Mulder (1996).

The MD process has been investigated for a long time and has many applications (RAMLOW, 2018), such as wastewater treatment (KIM *et al.*, 2015; KIM; LEE; CHO, 2016; MOKHTAR *et al.*, 2015), lithium recovery from aqueous solutions (QUIST-JENSEN *et al.*, 2016a), concentration of orange juice and whey (KEZIA *et al.*, 2015; QUIST-JENSEN *et al.*, 2016b), desalination (ADHAM *et al.*, 2013; CHUNG *et al.*, 2016; GONG *et al.*, 2021; GRYTA, 2016), arsenic-contaminated water treatment (CRISCUOLI; BAFARO; DRIOLI, 2013; MANNA; PAL, 2016) and ethanol recovery (TOMASZEWSKA; BIAŁOŃCZYK, 2016), among others.

Compared to other membrane separation processes, the main advantages of the MD process are (MADALOSSO, 2021):

- i. Possibility of complete removal of non-volatiles, salts, and ions resulting in a permeate of typical high purity;
- ii. Operating conditions are at low temperatures and pressures compared to traditional membrane separation systems (WANG; CHUNG, 2015);
- iii. Separation of salts is relatively constant during the process;
- iv. Rejection rate of salts, ions, and non-volatile compounds is practically independent of the feed concentration;

- v. Several types of alternative heating sources can be used to create the necessary operating temperature gradient, such as solar energy or the heat of the industrial effluent;
- vi. Generally, the feed source does not require extensive pretreatment (YE *et al.*, 2019);
- vii. No high mechanical strength is demanded for the membranes (WANG; CHUNG, 2015).

2.3.1 Configurations

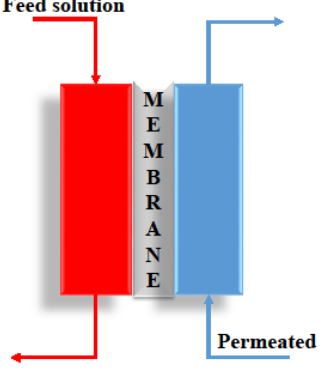
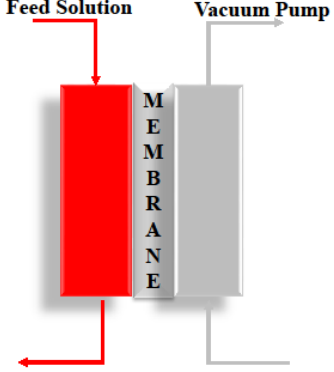
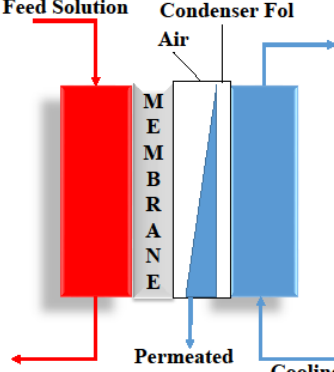
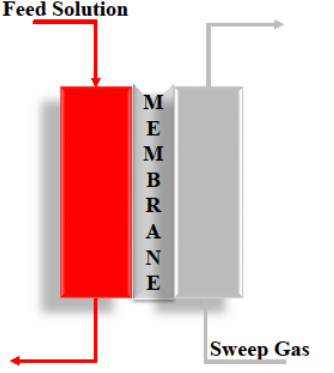
The MD process has four main configurations that vary the way to create the vapor pressure difference and the collection of permeate flux: Direct Contact (DCMD), Vacuum (VMD), Air Gap (AGMD), and Stripping Gas (SGMD) (RAMLOW, 2018). Figure 8 shows the four main DM configurations with their variations.

In the present work, the configuration applied is direct contact membrane distillation (DCMD), which is the most common and simplest configuration. However, there is a greater thermal loss in this configuration due to the accentuated effect of heat conduction caused by the temperature polarization which promotes the decrease in heat and mass flux. In this particular configuration, cooled water circulates tangentially to the membrane, thus inducing a driving force in the separation process (MADALOSSO *et al.*, 2021).

The main factors that determine the performance of a DCMD operation are design, configuration, and operating conditions. Removal capacity and productivity are directly altered according to the percolated path of the feed and permeate flow (countercurrent or concurrent), thermal and mechanical exchange media, and the physicochemical properties of feed and permeate. Among these DCMD operating and design parameters, the most relevant are the feed temperature and the membrane thickness (ASHOOR *et al.*, 2016; SANTOS, 2021).

DCMD has already been applied in several studies, such as treatments of textile wastewater contaminated with dyes (FORTUNATO *et al.*, 2021; RAMLOW; MACHADO; MARANGONI, 2017; TOLENTINO FILHO *et al.*, 2021), pharmaceutical wastewater (GUO *et al.*, 2020; MOZIA *et al.*, 2013), municipal sludge (KUMAR *et al.*, 2020; WU *et al.*, 2018), wastewater containing oily components (KALLA, 2021), saline waters (BONYADI *et al.*, 2022; GRYTA, 2016; TLILI *et al.*, 2022) and wastewater contaminated with heavy metals (ASIF *et al.*, 2021; KHRAISHEH; ALMOMANI; AL-GHOUTI, 2021; ZOLOTAREV *et al.*, 1994)

Figure 8- Conventional configurations of the membrane distillation process.

	<p>Direct contact membrane distillation (DCMD)</p> <ul style="list-style-type: none"> ➤ Simplest MD configuration; ➤ Membrane and liquid phases are in direct contact; ➤ Configuration with the biggest heat lossess;
	<p>Vacuum mebrane distillation (VMD)</p> <ul style="list-style-type: none"> ➤ Condensation occurs outside of the module; ➤ Highest permeate fluxes; ➤ Membrane is more prone to wetting
	<p>Air gap membrane distillation (AGMD)</p> <ul style="list-style-type: none"> ➤ Condensation is induced by the air insertion; ➤ Highest termal efficiency; ➤ Lower fluxes than DCMD;
	<p>Stripping gas membrane distillation (SGMD)</p> <ul style="list-style-type: none"> ➤ Condensation occurs outside the membrane module; ➤ An inert gas conduces the vapor to the condenser; ➤ Membrane lesser prone to wetting;

Ref: Adapted from Madalosso *et al.* (2021).

Analogous to DCMD configuration, Vacuum Membrane Distillation (VMD) presents as the driving force of separation-induced vacuum on the permeate side, causing vapor condensation outside the module. VMD has as characteristics lower operating temperatures and hydrostatic pressure; this configuration produces high permeate fluxes combined with low thermal loss. However, the membrane becomes more susceptible to wetting inside the pores (ABU-ZEID *et al.*, 2015).

Air Gap Membrane Distillation (AGMD) involves the insertion of an air gap between the membrane and the surface of the condenser, which acts as an insulating layer. The permeate flux becomes a direct function of temperature and feed flow and is inversely proportional to the thickness of the inserted air layer. This configuration increases the resistance to mass transfer across the membrane, which results in lower fluxes (SHAHU; THOMBRE, 2019).

Finally, Stripping Gas Membrane Distillation (SGMD) is a configuration where a cold inert gas is used to transfer water vapor to an external condenser. Process efficiency depends on temperature and feed and carrier gas flow; there is less thermal polarization in this module, as in VMD, permeate condensation also occurs outside the module (SAID *et al.*, 2020).

2.3.2 Membranes properties and operational conditions

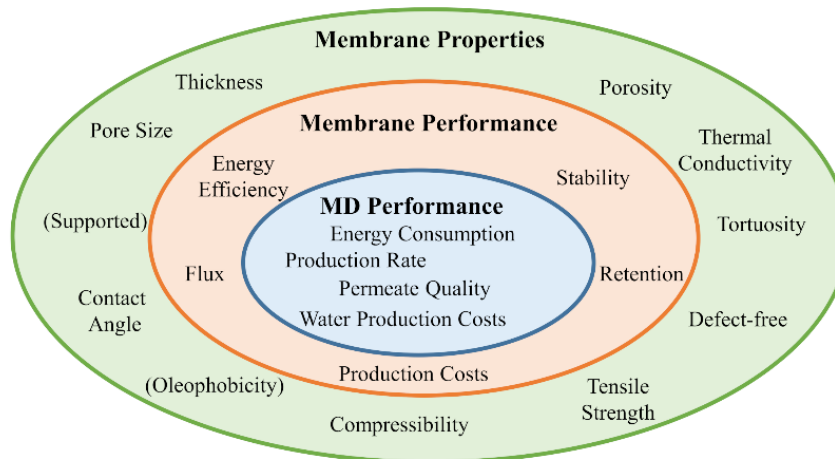
The structural properties of the membrane to be applied to membrane distillation must be optimized to achieve better performances of membrane use and, consequently better performances of the MD process as a whole, as exemplified in Figure 9. An adequate selection of microstructural properties in the membrane is fundamental for proper MD performance. Table 2 presents the key parameters that affect the MD process, as found in the literature, and recommendations for conventional uses.

The permeate flux in the MD process is determined by membrane porosity and pore geometry. Membranes with high porosity have a higher evaporation rate per unit of surface area. For this reason, the permeate flux is usually directly proportional to the open porosity of the material (ALKHUDHIRI; DARWISH; HILAL, 2012; EYKENS *et al.*, 2017).

Maximum pore size and average pore size are relevant parameters in determining a permeate flux. A high pore diameter promotes a high permeate flux, although this parameter requires a careful choice and evaluation (WOODS; PELLEGRINO; BURCH, 2011). High pore diameter values can make the system more susceptible to wetting (REZAEI *et al.*, 2018). According to Phattaranawik,

Jiraratananon and Fane (2003) influences of pore size distribution of large pore membranes tend to be negligible in some cases.

Figure 9- Evaluation criteria for membrane properties, membrane performance, and membrane distillation (MD) performance.



Ref: Adapted from Eykens *et al.* (2017).

Furthermore, in some cases it is interesting the presence of different pore diameter sizes, this could promote different diffusional and convective mass transfer mechanisms which could increase heat and mass flux (MADALOSSO *et al.*, 2021). In particular situations, membranes with a high average pore size are used (PHATTARANAWIK; JIRARATANANON; FANE, 2003).

The Liquid Entry Pressure (LEP), also known as the wetting pressure, is the minimum hydrostatic pressure required in the feed for water penetration into the membrane pores. LEP is directly related to the maximum pore size that the membrane has, and to the water contact angle of the membrane related to the material hydrophobicity (ALKHUDHIRI; DARWISH; HILAL, 2012).

Membrane thickness directly influences mass transfer, heat loss, and wetting. The greater the thickness, the more significant the mass transfer resistance, which can reduce permeate flux. On the other hand, a high thickness can improve heat exchange. An optimization of this factor is important for the proper functioning of the process (ALI *et al.*, 2016; EYKENS *et al.*, 2016a).

Table 2- Commercial values optimized for the membrane distillation process.

Property	Affects	Typical values (commercial)	Recommendations
Contact Angle (Θ)	Wetting resistance	80-160°	>90°, as high as possible
Liquid Entry Pressure (LEP)	Wetting resistance	0.5- 4.6 bar	>2.5 bar
Average pore diameter (d_{av})	Wetting resistance, flux and energy efficiency	0.012 – 1.2 μm	0.1 -1 μm
Porosity (ϵ)	Flux, energy efficiency, strength	38-90%	> 80%
Thickness (σ)	Flux, Energy efficiency, strength	10-200 μm	Low salinity: 30-60 μm High salinity 2-700 μm
Tortuosity (τ)	Flux, energy efficiency	1.1 – 3.9	As low as possible
Thermal conductivity (k)	Flux, energy efficiency	0.0031- 0.0057	As low as possible
Tensile Strength	Mechanical resistance	3.4 – 57.9 MPa	As high as possible
Compaction	Flux, energy efficiency, strength	PTFE: 22% at 0.6 bar	Not compressible

Ref: Adapted from Madalosso *et al.* (2021) and Eykens *et al.* (2017).

Therefore, the desirable properties for a fully functioning DCMD process are very broad, but these interdependencies must be considered. For example, an increase in membrane thickness can increase the tensile strength while decreasing mass transfer. High porosity allows high permeate flux;

however, high porosity combined with a high pore size makes the membrane more prone to wetting. Thus, criteria must be adopted in the production of membranes for the MD process to guarantee suitable overall process efficiency.

2.4 OVERVIEW

In summary, according to the literature review, biopolymers such as chitosan can be used for the development of different types of membranes, especially for membrane distillation. The diversification in the formation and correct structuring of pores' microstructure in chitosan can greatly increase productivity, flux, and selectivity (DELGADO-RANGEL *et al.*, 2020; SAHEBJAMEE *et al.*, 2020; SEDELKIN *et al.*, 2019).

Several researchers have already explored the generation of porosity in chitosan structures, whether in simpler techniques such as employing sacrificial materials (XU; HEIN; WANG, 2008; ZENG; RUCKENSTEIN, 1996), or in alternative methods such as freeze casting, electrospinning, or 3D printing (MURALI *et al.*, 2020; SAHRANAVARD *et al.*, 2020; SULTANA *et al.*, 2015). However, the latter is limited to producing large pores, which compromises a membrane's selectivity, making it technically unfeasible to efficiently produce submicron pores through these conformation routes. In this regard, Sahebjamee *et al.* (2020) developed a method using acetone as a second solvent in the traditional solvent casting process by solvent evaporation technique. In this case, the presence of acetone in the solution generated an increase in porosity and surface area. However, that work does not clarify the interaction of acetone with chitosan, as it uses other hydrophilic polymers after chitosan dissolution in the solvents. Moreover, it does not evaluate other chitosan mass fractions or optimize the water:acetone ratio for greater porosity generation.

Despite of the literature found on chitosan-based membranes in the pervaporation process, to the best of our knowledge, there is no published work on the use of chitosan as a membrane matrix in the membrane distillation (MD) process. This is still to be explored since pervaporation and membrane distillation use the same driving force. Similar works use chitosan as a coating on commercial PVDF membranes (AL-GHARABLI *et al.*, 2020; ARDESHIRI *et al.*, 2019). The main reason for this is the aforementioned difficulty in generating pores and the inherent moderate hydrophilicity for chitosan materials.

Therefore, our work focuses on two original aspects. Firstly, it seeks an improved development of pure chitosan membranes with higher porosity and a broad pore size distribution, then the application of a chitosan membrane to the membrane distillation process.

3 MATERIALS AND METHODS

The experimental units used in this work are located in the Laboratory of Process Control and Polymerization (LCP III and IV) of the Department of Chemical Engineering and Food Engineering (EQA) of the Federal University of Santa Catarina (UFSC). However, the characterization equipment is allocated in different research laboratories due to the multidisciplinary nature of the work. Among the partner departments and laboratories are: the Central Laboratory of Electronic Microscopy (LCME), the Analysis Center at EQA/UFSC, and the Interdisciplinary Laboratory for the Development of Nanostructures (LINDEN).

To facilitate understanding, this Chapter is divided into 4 sections: materials, membrane synthesis, membrane characterization, and membrane performance tests.

3.1 MATERIALS

The reagents used in all preparations, purifications, and characterizations are of analytical purity and were purchased from commercial sources, and have not undergone prior purification. The synthesis of the membranes used medium molar mass commercial chitosan powder as a solid base material (Sigma-Aldrich, MM: 190-310 kDa, DD 75-85%), glacial acetic acid as an additive (Sigma-Aldrich), and acetone as a non-solvent (Exodo Científica, purity >99%). Deionized water (SPlabor) was used as a solvent in the production of membranes and to characterize contact angle and degree of swelling. Analytical grade potassium bromide (KBr) pellets were employed for Fourier Transform Infrared (FTIR) analysis.

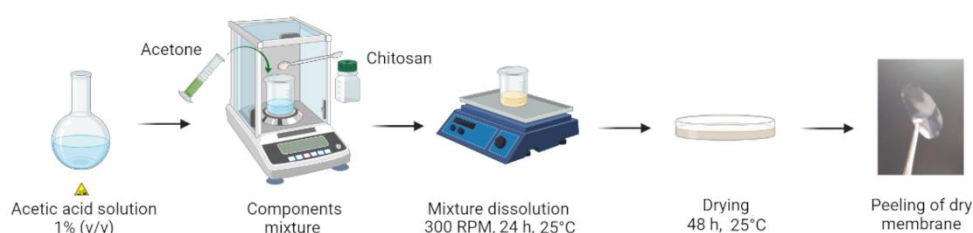
3.2 MEMBRANE SYNTHESIS

For the preparation of the membranes, the experimental route was based on Sahebjamee *et al.* (2020). First, samples with different compositions of chitosan content in mass fraction, in relation to total solvent mass, and different solvent volume ratios (water/acetone) were tested, as shown in Table 3.

Table 3- Overview of materials used.

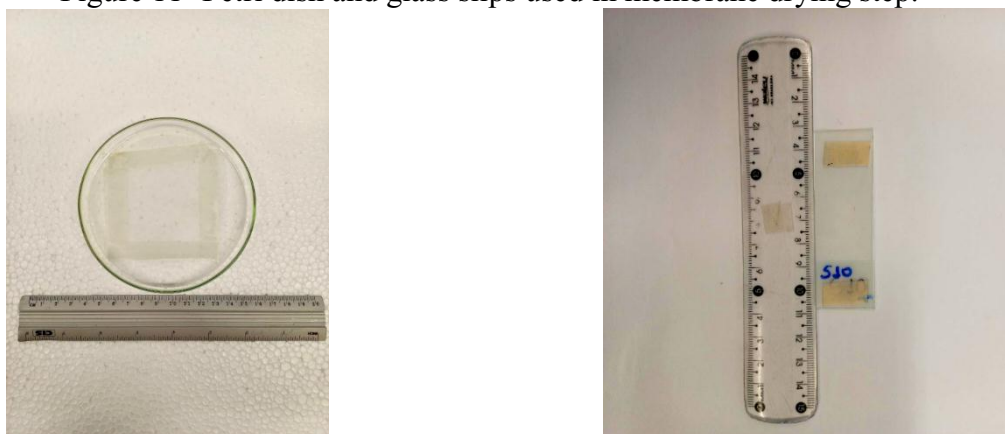
Component	Function	Amount
Chitosan powder	Matrix	0.5 - 2.0 wt%
Water (S1)	Solvent	Volume ratio S1:S2 (1:0 - 9:1)
Acetone (S2)	Non-solvent	
Acetic acid	Additive	1.0 wt% in water (S1)

The experimental preparation consists of four steps and is shown in Figure 10. First, a diluted solution of acetic acid was prepared in water at a fixed concentration of 1% (v/v). The second step consists of mixing all components: first, the desired amounts of acetone are added, and then the chitosan content is placed in the system; samples without the acetone addition were tested as a control. The third step consisted of magnetic stirring of the system at room temperature (25 ± 2 °C) for 24 h until the solution was as homogeneous as possible. However, due to the partial solubility of chitosan, a fraction of insoluble matter always persists in the bulk medium. The last step is drying, which takes place at room temperature for 48 h in a fume hood with a relative humidity of ~60%. To facilitate the process of removing the dry membrane, a polyester terephthalate film (Mylar[®]) was glued with a double-sided adhesive tape and used on glass supports for the two units tested to produce the membrane (Petri dish and glass coverslips), as shown in Figure 11.

Figure 10- Process scheme of chitosan membrane (made with Biorender[®]).

Ref: Author (2022).

Figure 11- Petri dish and glass slips used in membrane drying step.



Ref: Author (2022).

According to the increase in acetone added, a solubility limit is associated with a limit volume ratio. This threshold value corresponds to a 1:1 water:acetone value with 0.5 wt% chitosan, 2:1 with 1.0 wt% chitosan and 3:1 with 2.0 wt%. Any attempt to incorporate a greater amount of acetone in the dispersion of the respective system generates a very intense phase separation.

3.3 MEMBRANE CHARACTERIZATION

3.3.1 Contact angle, swelling index, and open porosity

Membrane wettability, its modifications with chitosan content, and the presence and amount of acetone were determined through apparent surface contact angle analysis. The contact angle was measured using a goniometer (Ramé-Hart model 250-F1) coupled with image processing software (DROPIimage Advanced). The inserted volume of each drop on the membrane surface was approximately 10 μL , and 3 measurements for each sample were performed randomly to produce an average value. This apparent surface contact angle was determined with the dry membranes.

The Swelling Index (SI) was investigated for different membrane compositions. The determination was performed by immersing dry pre-weighed samples in distilled water at room temperature for 48 h. After immersion, the membranes were gently set on absorbent paper to remove excess and then weighed at saturation. The experiments were performed in triplicate, and the results are presented as mean value \pm standard deviation. Equation 1 shows how SI (%) was calculated:

$$\text{SI (\%)} = \frac{M_w - M_d}{M_d} \times 100 \quad (1)$$

where M_w and M_d are the masses (g) of the wet and dry membrane samples, respectively.

Analogously to Equation 1, the open porosity (P , in %) can be estimated by expanding Equation 1 into Equation 2:

$$P (\%) = \frac{\left[\frac{M_w - M_d}{\rho_{H_2O}} \right]}{\left[\frac{M_w - M_d}{\rho_{H_2O}} \right] + \frac{M_d}{\rho_{chi}}} \times 100 \quad (2)$$

where ρ_{H_2O} is the density of water at room temperature (0.998 g/cm^3) and ρ_{chi} is the density of chitosan powder (1.5 g/cm^3) given by the literature (PICKER-FREIER; BRINK, 2006).

3.3.2 Fourier-transform infrared spectroscopy (FTIR)

A Fourier Transform Infrared Spectroscopy (FTIR) analysis was performed (Shimadzu, IR-Prestige) to investigate the effect of acetone on the chemical structure of membranes. The chitosan powder and blank samples were prepared in pellets with potassium bromide (KBr) followed by drying at room temperature before reading. Since the chitosan membranes already have a film shape, they were firstly dried at room temperature and then directly analyzed in the spectrophotometer. All samples were evaluated in the wavelength range from 4000 to 500 cm^{-1} .

The Deacetylation Degree of chitosan (DD in %) was also determined by FTIR using Equation 3 which is an empirical correlation (DOMSZY; ROBERTS, 1985) and has been strongly applied to chitosan-derived materials (BASKAR; KUMAR, 2009; RUPIASIH *et al.*, 2017; SAHEBJAMEE *et al.*, 2020) to avoid using more expensive and time-consuming techniques such as NMR or elemental analysis:

$$DD (\%) = 100 - \left(\frac{A_{1665}}{A_{3450}} \right) \times \left(\frac{100}{1.33} \right) \quad (3)$$

where A_{1655} is the absorbance at 1655 cm^{-1} corresponding to the C=O stretch of the amide group and A_{3450} is the absorbance at 3450 cm^{-1} corresponding to the O-H stretch of the hydroxyl group. Absorbance ratio values were determined using the baseline method.

3.3.3 X-ray Diffractometry

Membrane spectra were obtained by X-ray Diffractometry (XRD, Rigaku MiniFlex600) with a scintillation counter detector (K β filter), using CuK α radiation ($\lambda = 1.5418 \text{ \AA}$), and 40 kV. The samples of chitosan powder and membranes were analyzed in a range of 5-60°, following a step of 0.02° at a rate of 5°/min.

The Crystallinity Degree (CD in %) of chitosan was also determined by using Equation 4:

$$\text{CD (\%)} = \left(\frac{I_{110} - I_{\text{am}}}{I_{110}} \right) \quad (4)$$

where I_{110} is the maximum height of the crystalline peak and I_{am} is the height of the amorphous peak in the same spectrum. A peak deconvolution analysis process was applied (OriginPro® 8.5 software library).

3.3.4 Differential scanning calorimetry

Differential Scanning Calorimetry (DSC) measurements were performed to characterize the membranes and chitosan precursor powder in terms of degradation temperature (T_{onset}) and glass transition temperature (T_g). Solid samples with masses between 1 and $3 \pm 1 \text{ mg}$ were sealed in aluminum capsules and analyzed (Jade-DSC, Perkin Elmer). First, a heating and cooling curve was performed. The first run started with heating from 25 to 110 °C at 10 °C/min, followed by cooling down to 25 °C at 10 °C/min. The second run was performed with heating from 25 to 480°C at 10 °C/min. The T_g of the materials was determined through the average value of the inflection region of the calorimetric curve, while the T_{onset} was defined as the initial temperature where the degradation peak of the samples begins.

3.3.5 Nitrogen adsorption and desorption porosimetry

The procedure using the BET method was carried out in the Central Analysis, EQA UFSC. The porosimeter equipment employed were from Quantachrome (Quantoorb, Quantachrome). This technique is based on gas adsorption and desorption, with nitrogen gas adsorbed onto a solid sample.

Physisorption tests were carried out on nitrogen gas at 77K, in relative pressures of 0.0-1.0 atm. The samples were previously degassed with temperature of 200°C and 30°C, under vacuum (10 to 7 torr).

The curve relating the amount of adsorbed gas at equilibrium and the pressure of the gas at constant temperature is called the adsorption isotherm. Different isotherms are related to different types of pore size. Similarly, if present, hysteresis is also related to the shape and morphology of the pores.

3.3.6 Field emission gun scanning electron microscopy

Field Emission Gun – Scanning Electron Microscopy (FEG-SEM, JEOL® JSM-6701F) analyses of the membrane surface were performed. The previously dried membranes were attached on top of metallic stubs. Before using the equipment, the membrane samples were sputtered with gold (CED 030, Baltec). In the images obtained, the morphological characteristics of the membrane surface were observed to verify the influence on the solid's content and the ratio of solvents used in their formulation.

3.4 MEMBRANE PERFORMANCE TESTS

The Direct Contact Membrane Distillation (DCMD) experiments were carried out to evaluate porous chitosan membrane performance, as represented in Figure 12. The recirculate flow rates were 1.5 L min^{-1} for the hot feed stream and 0.7 L/min for the cold permeate stream. The feed temperature was controlled at $60 \text{ }^\circ\text{C}$, and the permeate was set at $20 \text{ }^\circ\text{C}$. Those experimental conditions were based in previous work from literature from commercial MD membranes (RAMLOW, 2018; RAMLOW *et al.*, 2019; SRISURICHAN; JIRARATANANON; FANE, 2006; TOLENTINO FILHO *et al.*, 2022).

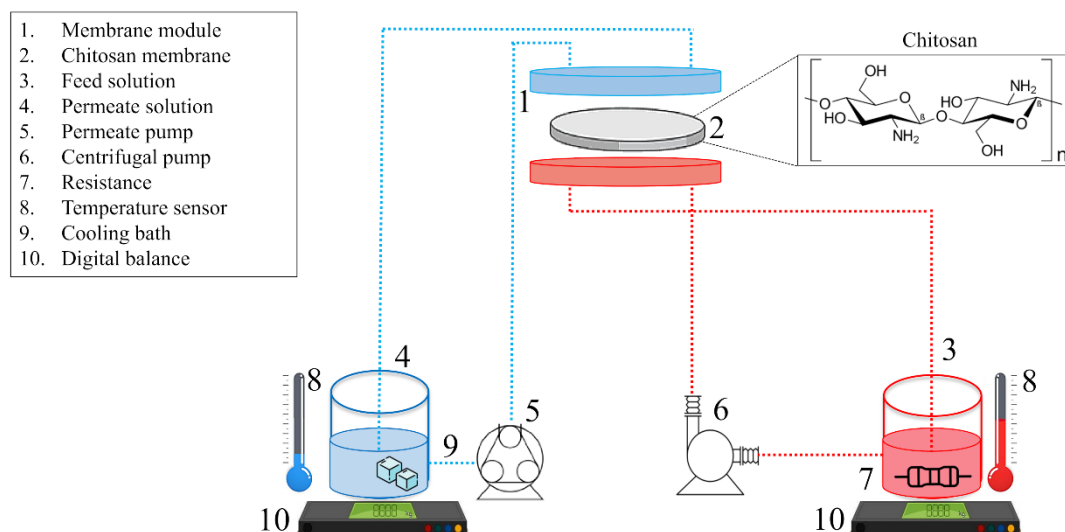
The volumes of feed (distilled water) and permeate (distilled water) were, respectively, 2 L and 0.6 L, and both streams were recirculated in counter current. First, as a comparison between the membranes, the time for each experiment was 1 h, followed by a longer period (2.5 h) for the higher flux membrane obtained.

The DCMD permeate flux for each membrane was determined by the rate of change of permeate mass. The permeate flux (J , $\text{kg}\cdot\text{m}^{-2}\cdot\text{h}^{-1}$) was determined by Equation 5:

$$J = \frac{M_t - M_{t_0}}{A \times t} \quad (5)$$

where M_t and M_{t_0} are the permeate masses (kg), A is the effective area of membrane (m^2), and t is the time duration (h). The effective membrane area was 0.0013 m^2 .

Figure 12- Schematic of direct contact membrane distillation (DCMD) setup used to quantify the flux of water vapor transported across porous chitosan membranes.



Ref: Author (2022).

The centrifugal pump flows the solution from the feed to the unit, while the submerged pump in the permeate tank pumps this solution. The supply temperature is controlled using an electrical resistance and a commercial controller. Four digital thermometers at the inputs and outputs of the two streams (cold and hot) indicate the temperature values. The module is made of stainless steel, composed of two identical bases that fit together and have perforated membrane support. A small module was used with an internal diameter of 5.2 cm, and the rings are attached to the bases. Figure 13 shows a photograph of the module used. The chitosan membrane is inserted onto the support between the two module bases. Polymer rings (PTFE and Nylon) are used to help seal the module during experiments.

For the Liquid Entry Pressure (LEP) measurements, compressed air was used to generate the applied pressure, and a regulating valve made its control. The effective pressure was measured using a manometer connected next to the membrane module to avoid the pressure drop through the pipe. The LEP measurement follows three main steps (SILVA *et al.*, 2021b): 1) the distilled water was put into the membrane module; 2) pressure of 0.2 bar was applied on the membrane surface and maintained for 10 min to obtain a homogeneous liquid pressure, and 3) the pressure was increased by 0.2 bar every 5 min until achieving the LEP. When the pressure exerts the maximum pressure of the liquid under the membrane, the solution penetrates inside the membrane pores, causing the wetting.

Therefore, the pressure value at which the first drop of distilled water was observed on the permeate side was considered the LEP value.

Figure 13- Images of the membrane module applied.



Ref: Author (2022).

4 RESULTS AND DISCUSSION

In this chapter, the experimental results obtained in the development of this thesis are presented. In Section 4.1, the influence of acetone on the solubility with chitosan is discussed. Sections 4.2, 4.3, 4.4, 4.5 and 4.6 present the membrane characterization results obtained regarding membrane properties. Finally, Section 4.7 presents the membrane performance results for the MD system.

4.1 SYSTEM SOLUBILITY

According to Roberts (1992), who discussed the solubility of chitin and chitosan, chitosan is very poorly soluble in organic solvents. However, if the chemical structure of the solvent has a small carbon chain, chitosan can tolerate 40-50% by volume of solvents such as acetone. The results obtained corroborate this statement, although insoluble particulates in the dissolution process always persist.

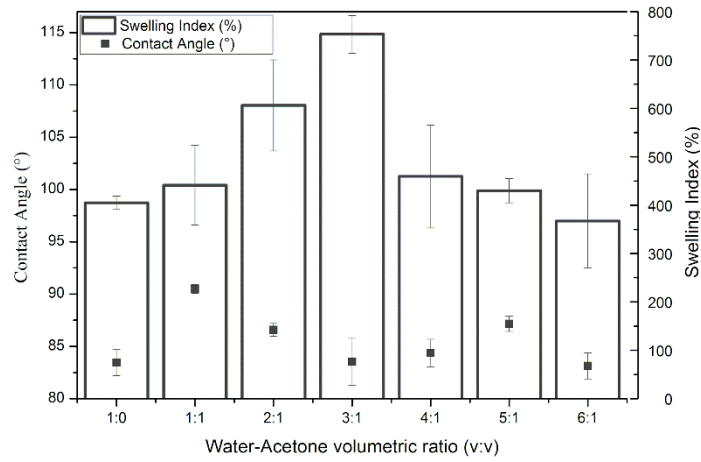
It was not possible to obtain the same water:acetone volume ratio used by Sahebamee *et al.* (2020), 2:1 with 2.0 wt% of chitosan, mainly due to the difference in the raw material of chitosan powder applied. The solubility limit value depends on several variables, such as the intrinsic physical and chemical properties of chitosan (molar mass, degree of deacetylation, viscosity, density), as well as processing factors (temperature, type of agitator, frequency of agitation, presence of surfactants), among other parameters.

For this reason, the present work used chitosan of medium molar mass. According to Roy *et al.* (2017), chitosan has a solubility in water inversely proportional to its molar mass. Although the chitosan used does not have as high solubility as the low molar mass, the selected raw material has better stability for application after the synthesized membrane. Post-drying treatments with NaOH, which are widely used in several works in the literature, are also avoided to dismiss further changes in the membrane microstructure (LLANOS; VERCİK; VERCİK, 2015). The use of glutaraldehyde or other crosslinking agents was also avoided to not promote a decrease in pore size and open porosity (WANG *et al.*, 2006).

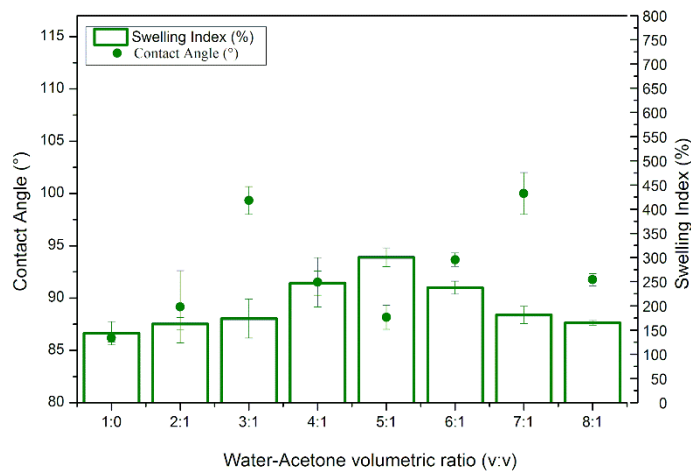
4.2 MEMBRANE WETTABILITY AND POROSITY

Figure 14 shows the contact angle results in water and the swelling index of all membranes tested according to the variation in the volume ratio of water:acetone and solids content. The results show different values according to the solids content used, the presence of acetone and the volume of water:acetone ratio used.

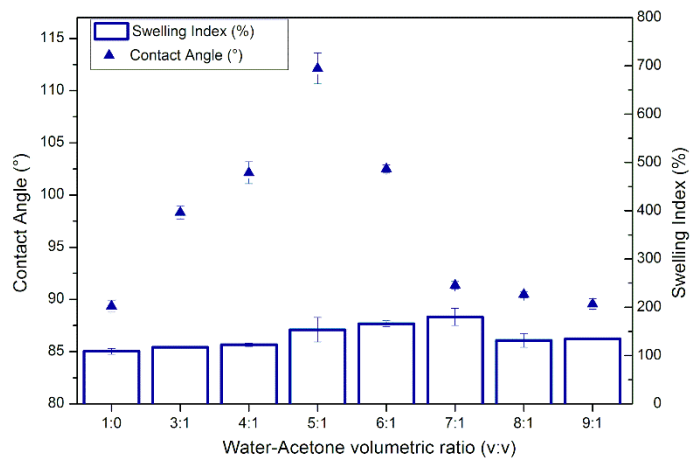
Figure 14- Contact angle and swelling index for chitosan membrane according to water:acetone ratio and chitosan amount: (a) 0.5 wt% , (b) 1.0 wt%, and (c) 2.0 wt%.



(a)



(b)



(c)

Ref: Author (2021).

As the mass fraction increases, the greater the contact angle tendency and also the lower the degree of swelling of the membranes. It is possible to notice that in the lower solid fraction, there is higher swelling index with lower contact angle variation. In other hand, for the 2.0 wt% membranes the tendency is the opposite and consequently the highest membranes hydrophobicity are obtained. Finally, the water:acetone volume ratio employed promotes a maximum swelling degree point. This value corresponds to a difference amount according to the solids content from 3:1 to 0.5 wt%, from 5:1 to 1.0 wt% and from 7:1 to 2.0 wt%.

The swelling index is one of the most important properties of chitosan films and membranes, which can represent the viability of chitosan for a biomedical application (BASKAR; KUMAR, 2009). This water uptake absorption capacity is related to the intrinsic hydrophilicity nature of the chitosan membrane (CUI; BEACH; ANASTAS, 2011), chain crosslinking (CADOGAN *et al.*, 2016), availability of amino groups on the surface to participate in hydrogen bonding (MARQUES *et al.*, 2019; WAN *et al.*, 2003), open porosity (SAHEBJAMEE *et al.*, 2020), and average pore size (CHEN *et al.*, 2007). Moreover, these factors can correlate with each other and change the degree of swelling as a whole (CADOGAN *et al.*, 2016). Rupiash *et al.* (2017) obtained the same swelling index results of the present work for 1 and 2 wt% of pure chitosan membrane in the same water and acetic acid content, but without acetone, even using chitosan with high molar mass (900 kDa) as precursor material. The authors also realized that the increase in solids content in the membrane formation provided a gain in swelling degree values, which were related to the pore density or open porosity in the sample.

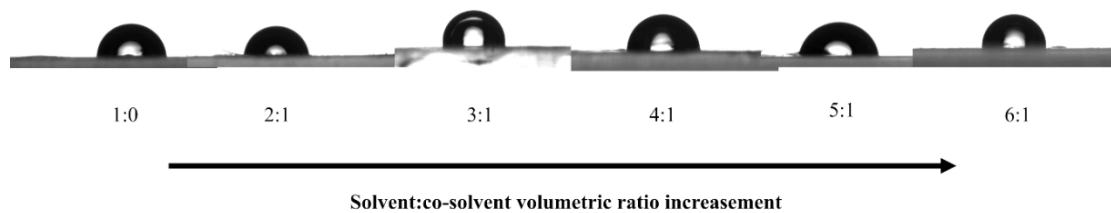
Therefore, it is possible to extrapolate the concept to the present work and show that the increase in the degree of swelling associated with the volume water:acetone ratio used may be associated with the increase in the open porosity of the system. Sedelkin *et al.* (2019) also stated that this decrease in swelling with increasing chitosan concentration might be associated with the low porosity of the membrane obtained, which causes a reduction in the penetration rate of dissolving agents and inaccessibility of polymeric macromolecular chains and surface functional groups.

Figure 15 shows the image obtained for the 1 wt% curve of chitosan with its variation in solvent composition. With these results, it is possible to observe the hydrophilicity variation of the system. The results show a contact angle variation of approximately 83-112° representing a moderately hydrophobic, being a favorable behavior in the membrane distillation process.

Membranes tend to have little increase or change in hydrophobicity as the solids content increases in samples without acetone, but combined with the presence of the other solvent, there are

greater increases in contact angles according to volumetric ratio variations, especially in samples with 2 wt%. At the maximum swelling index for each mass concentration of chitosan applied, there is a point of the minimum relative contact angle by the neighborhood of volumetric ratios.

Figure 15- Contact angle image for membrane containing 1 wt% chitosan with the increase of water:acetone solvent ratio.

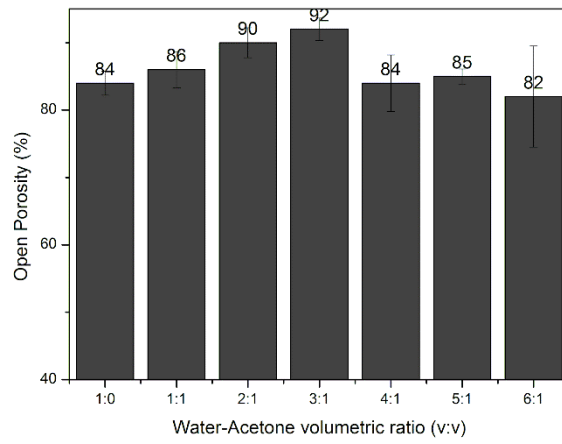


Ref: Author (2021).

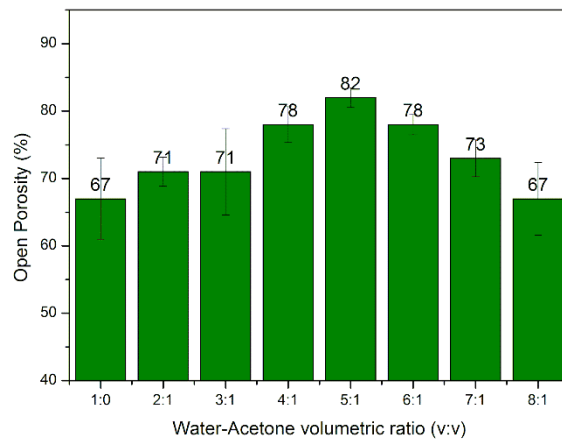
In the literature, the typical contact angle values of water in pure chitosan films and membranes have been reported in the range of 76-104° (CAMPOS *et al.*, 2009; KIM *et al.*, 2009; ZHAO *et al.*, 2009). Variations in the contact angle are common depending on the solvent applied and its concentration on the adopted mass fraction (CUI; BEACH; ANASTAS, 2011). Thus, some works have developed superhydrophilic ($\Theta < 5^\circ$) or superhydrophobic ($\Theta > 150^\circ$) chitosan membranes depending on the materials applied as raw material and membrane synthesis conditions without first thinking about a post-synthesis functionalization (CAMPOS *et al.*, 2009; SONG *et al.*, 2010).

Marques *et al.* (2019) reported that lower hydrophilicity with textural change occurred during the film formation phase in the material drying step. The authors also observed a decreasing effect on the surface amino functional groups of chitosan, leading to a blockage in water permeation. Furthermore, an increase in contact angle values may be associated with a surface with lower open porosity. Therefore, several factors can influence the contact angle of a chitosan membrane, among them the surface roughness, the presence of amino groups, and the open porosity. These factors can explain the relative contact angle increases with the increase in the mass concentration used in the present work. The variations in contact angle related to the water:acetone volume ratio (Figure 15) are strongly associated with variations in the swelling index in water and open porosity (Figure 16). When there is eventually a greater swelling index and consequently a greater open porosity, water percolation becomes faster.

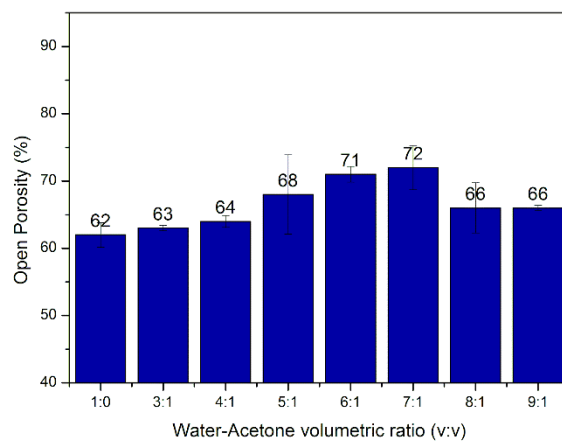
Figure 16- Open porosities of the chitosan membranes according to the water:acetone ratio and chitosan amount: (a) 0.5 wt%, (b) 1.0 wt% and (c) 2.0 wt%.



(a)



(b)



(c)

Therefore, the relative minimum contact angle is presented together with the absolute maximum degree of swelling for each mass fraction. However, volumetric ratios of acetone greater than the ratios of the maximum degree of swelling end up decreasing the water absorption and significantly increasing the contact angle values, possibly due to the residual presence of organic solvent and interactions with the surface functional groups of chitosan.

The open porosity results in Figure 16 show the same behavior as the swelling index results. The values obtained are in the range of 62-92%, which are suitable for the membrane distillation process. Optimized acetone conditions produce, compared to shaped membranes without acetone, a percentage gain of 9.52% for samples containing 0.5 wt%, 22.38% for 1.0 wt% and 16.12% for 2.0 wt% chitosan. These results demonstrate the importance of the presence of acetone in the production of the membrane microstructure and also reinforce the importance of optimizing the amount of acetone used for maximum porosity gain and better subsequent flow results.

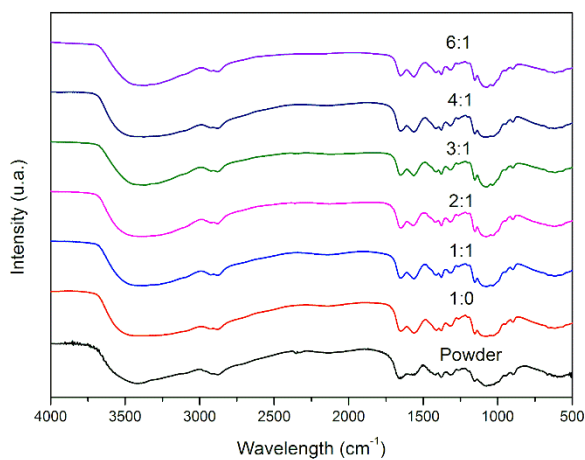
Evaluating the open porosity of chitosan membranes using the solvent evaporation technique, the literature reports that the open porosity of chitosan membranes tends to decrease as the molar mass of the precursor chitosan increases and also when the solids content used is increased (SEDELKIN *et al.*, 2019). Therefore, compared to the work by Sahebamee *et al.* (2020), there was the generation of an open porosity of 60% with a water:acetone volume ratio of 2:1 and a mass concentration of 2.0 wt% chitosan of 130 kDa. Similarly, the present work has a maximum porosity of 72% in the same mass concentration range, even using chitosan of 190-310 kDa, proving the importance of the selection of the volume water: acetone ratio to be used to produce a membrane with higher porosity. In the present work, the highest porosity value obtained was 92% for the membrane containing 0.5 wt%.

4.3 CHEMICAL AND CRYSTALLOGRAPHIC PROPERTIES

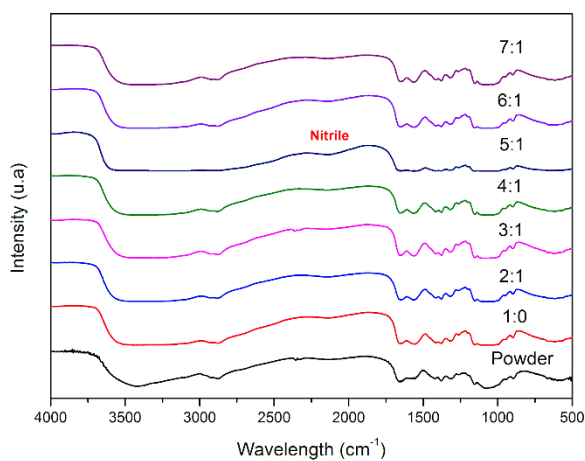
The FTIR spectra of all membranes evaluated, as well as their characteristic functional groups, are shown in Figure 17, and Table 4. The results obtained represent well the characteristic peaks of chitosan (RUPIASIH; SUMADIYASA; PUTRA, 2017) and also demonstrate the dependence of the mass concentration of chitosan in the FTIR spectra.

By analyzing the spectra, the transmission band seen in the chitosan powder sample at 3450 cm^{-1} belongs to the $-\text{OH}$ groups of the polymeric structure. From Figure 17, it was observed that as the synthesis of the membranes occurs, the amplitude of this band also changes and changes its position.

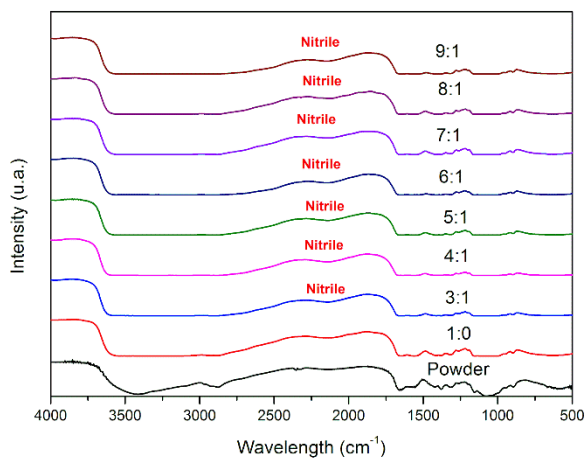
Figure 17- FTIR spectrum of the chitosan membranes and powder according to water:acetone ratio and chitosan amount: (a) 0.5 wt%, (b) 1.0 wt% and (c) 2.0 wt% .



(a)



(b)



(c)

Ref: Author (2021).

The characteristic peak at 2884 cm^{-1} is related to the stretching of the $-\text{CH}$ bond of chitosan, which has a small change in frequency according to solids content and water: acetone volumetric ratio. The third relevant peak is at 1655 cm^{-1} , which corresponds to the amide bond stretch ($\text{C}=\text{O}$), and was strongly altered concerning solids content and acetone volumetric ratio. This indicates a tendency to convert amino groups (RNH_2) into acetamido groups (RNHCOCH_3) as the solids content increases and the acetone ratio used is optimized.

In some curves of the samples with 1.0 and 2.0 wt% at 2250 cm^{-1} , it is also possible to notice the presence of nitriles ($\text{C}\equiv\text{N}$) in the points of maximum porosity and degree of swelling already obtained, indicating a possible reaction between the amino groups of chitosan and the carbonyl groups of acetone.

Osório *et al.* (2016) also reported the same behavior at the peaks 2250 cm^{-1} and 1655 cm^{-1} , as the present work in a reaction of mixing chitosan with acetyl-acetone. Those authors attributed this behavior to the incorporation of the carbonyl of acetone used in the structure of the chitosan.

Table 4- The main bands obtained in chitosan membranes after FTIR analyses.

Peak	Frequency	Intensity	Type of Vibration	Type of Bond	Functional Group
3500-3650	All	Strong	Stretching	O-H	Alcohols
2884	Mostly	Strong/Weak	Stretching	C-H	Alkanes
2250	Some	Weak	Stretching	$\text{C}\equiv\text{N}$	Nitriles
1655	All	Mostly Strong	Stretching	$\text{C}=\text{O}$	Amide
1570	Some	Strong	Stretching	N-O	Nitro Compound
1414	Some	Medium	Bending	C-H	Alkanes
1370	All	Medium	Bending	O-H	Alcohols
1250	All	Weak	Stretching	C-N	Amine
900, 1020 and 1155	All	Strong	Stretching/Bending	-	Saccharide Structures

Ref: Author (2021).

Therefore, knowing that physical drying phenomena do not usually change the intensity or generate the appearance of new peaks in FTIR spectra (ARANTES *et al.*, 2014), it is possible to conclude that a chemical reaction is associated with the presence of acetone in the membrane

composition. However, more studies must be carried out to propose a correct structure and reaction mechanism to understand the final chemical structure achieved.

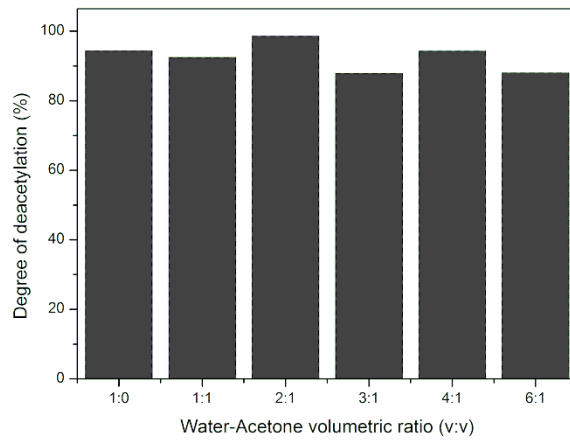
Figure 18 shows the degree of deacetylation for all membranes studied from the absorbances obtained by the FTIR analysis. Equation (3) is an empirical correlation (DOMSZY; ROBERTS, 1985) and has been strongly applied to chitosan-derived materials (BASKAR; KUMAR, 2009; RUPIASIH *et al.*, 2017; SAHEBJAMEE *et al.*, 2020; ZAWADZKI; KACZMAREK, 2010) to avoid using more expensive and time-consuming techniques such as NMR or elemental analysis. Domszy and Roberts (1985) proved that the use of the 3450 cm^{-1} absorption band as an internal standard in the determination of the extent of N-acetylation of chitosan from the absorbance of the amide I band at 1655 cm^{-1} has been shown to be justified. The correlation obtained are relatively insensitive to the presence of small amounts of adsorbed water.

The Degree of Deacetylation (DD) obtained by Equation 3 for the FTIR curve of the chitosan powder sample was 76.56%, consistent with what was reported by the manufacturer (DD: 75-85%). On the other hand, the degree of deacetylation in the membranes did not remain constant. The control samples without acetone (1:0) for all mass concentrations showed higher values than the chitosan powder sample. Knowing that an increase in the degree of deacetylation is not thermodynamically favorable (BASKAR; KUMAR, 2009), reference values greater than 76.56% must be more associated with the loss of insoluble materials in the conformation of the membranes.

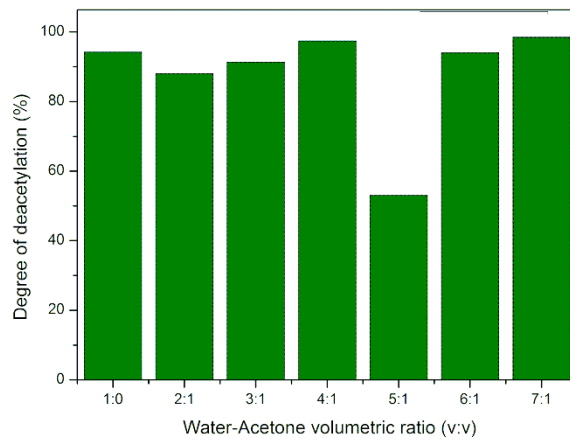
In Figure 18, it is also possible to see a tendency for the DD to fall to a relative minimum value at the maximum points of the swelling index and open porosity for each curve (3:1 for 0.5 wt%; 5:1 for 1.0 wt% and 7:1 to 2.0 wt% chitosan). Particularly, the values in the 1% and 2% curves tend to have DD values much lower than the reference chitosan powder sample. These values, together with the FTIR spectra, may indicate a possible chemical interaction of the amino groups (RNH_2).

In this case, they would be converting into acetamido radicals (RNHCOCH_3) and thus an acetylation reaction would occur. Kim *et al.* (2004) also associate a decrease in the degree of deacetylation of chitosan through a chemical reaction of the amino groups with acetic acid at high temperatures for drying. However, further studies are needed to propose the mechanism of action of chitosan more accurately with the presence of acetone in its conformation in its different volume water:acetone ratios. It is possible to conclude that the action of acetone against the functional groups of chitosan is a function of the mass concentration of the system, and the volume water:acetone ratio used. Furthermore the decrease in amino groups may be associated with increases in the contact angle present in 1 and 2 wt% chitosan, as already explained in Figure 14-15.

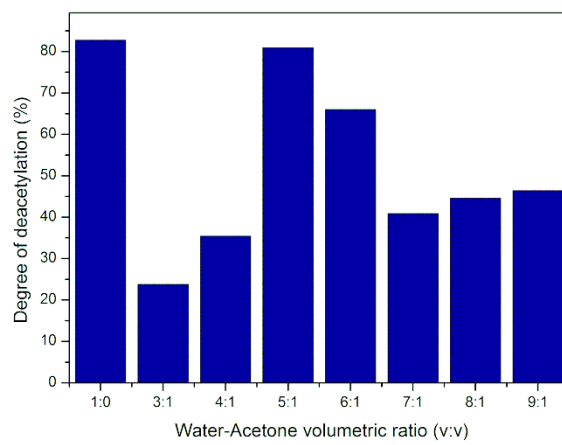
Figure 18- Degree of deacetylation from FTIR spectrum data for the chitosan membrane according to the water:acetone ratio and chitosan amount: (a) 0.5 wt%, (b) 1.0 wt% and (c) 2.0 wt%.



(a)



(b)

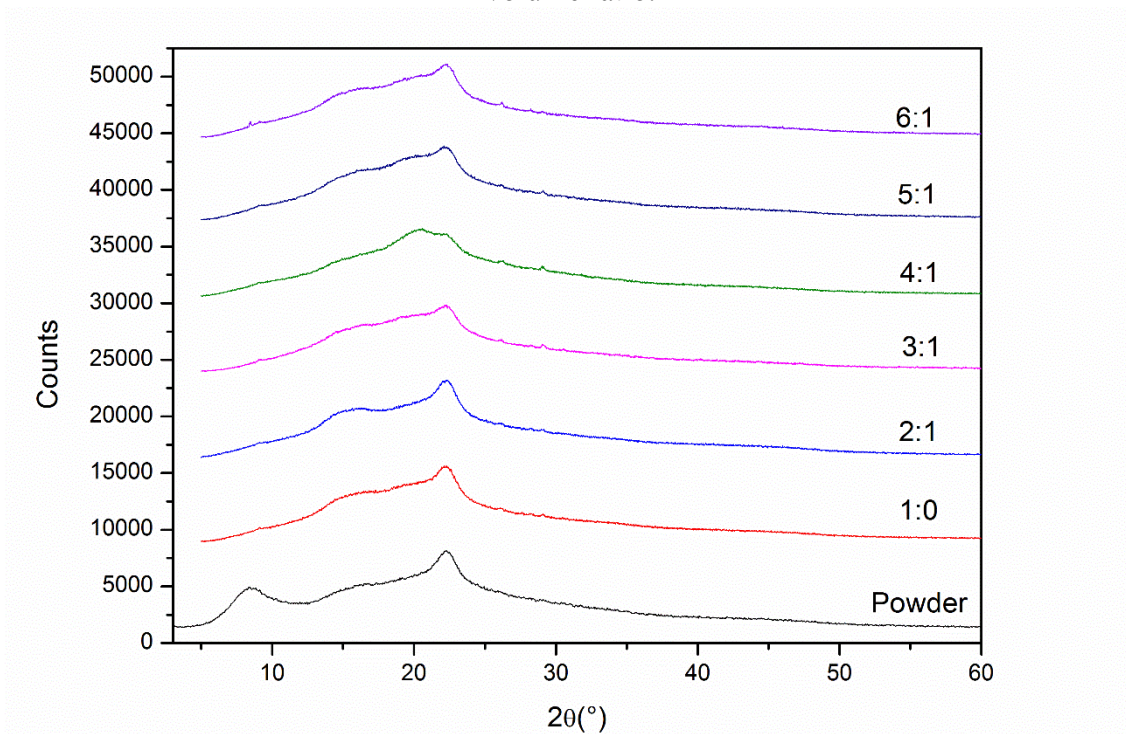


(c)

Ref: Author (2021).

XRD spectra for chitosan powder and the chitosan membranes containing 1 wt% chitosan as the volume water:acetone ratio increases are presented in Figure 19. The crystallinity index (CI) obtained from the XRD spectra are presented in Table 5. The other spectra in Table 5, which were not represented in Figure 19, are found in Figure A1 (Appendix).

Figure 19- XRD spectra for the membrane containing 1 wt% with the increase of water:acetone volume ratio.



Ref: Author (2021).

In Figure 19, it is possible to perceive the crystallographic changes of chitosan powder for its conformation in membranes, and that all of the samples present semicrystalline polymer structures. Chitosan has this profile due to strong intra and intermolecular interactions, characterized by the hydrogen bonds formed between the functional groups on the biopolymer's surfaces, and many authors attribute the amorphous peak to water absorbed in the polymeric structure (ARANTES *et al.*, 2014; RUPIASIH; SUMADIYASA; PUTRA, 2017).

In the powder precursor sample, an amorphous peak centered at approximately 9° can be seen, and this peak shifts to approximately 15° in membrane conformations and also increases its width, becoming less noticeable. According to Llanos, Vercik e Vercik (2015), the modification of this first orthorhombic peak is related to the change in crystallite morphology in the chitosan polymer network connected with the loss of hydrogen bonds and deprotonation of amino groups.

The crystallinity index presented in Table 5 shows a slight decrease between the powder sample and the membranes, but little change between solids content and water: acetone ratio used, all values remaining between 0.26 - 0.30.

Table 5- Crystallinity Index for some selected chitosan membranes.

Sample	Chitosan Amount (wt%)	Water:Acetone volume ratio (v:v)	Cristalinity Index
Powder	-	-	0.40
1		1:0	0.30
2		2:1	0.31
3	1.0	3:1	0.26
4		4:1	0.30
5		5:1	0.26
6		6:1	0.29
7	0.5	1:0	0.30
8		3:1	0.28
9	2.0	1:0	0.30
10		7:1	0.24

Ref: Author (2021).

According to the literature, it is known that the crystallinity index of chitosan films is strongly associated with the method of preparation, microstructural morphological characteristics of the system, thermal properties, and degree of deacetylation (BASKAR; KUMAR, 2009; DELEZUK; PAVINATTO; CAMPANA FILHO, 2014; RODRIGUES, 2018; SEDELKIN *et al.*, 2019).

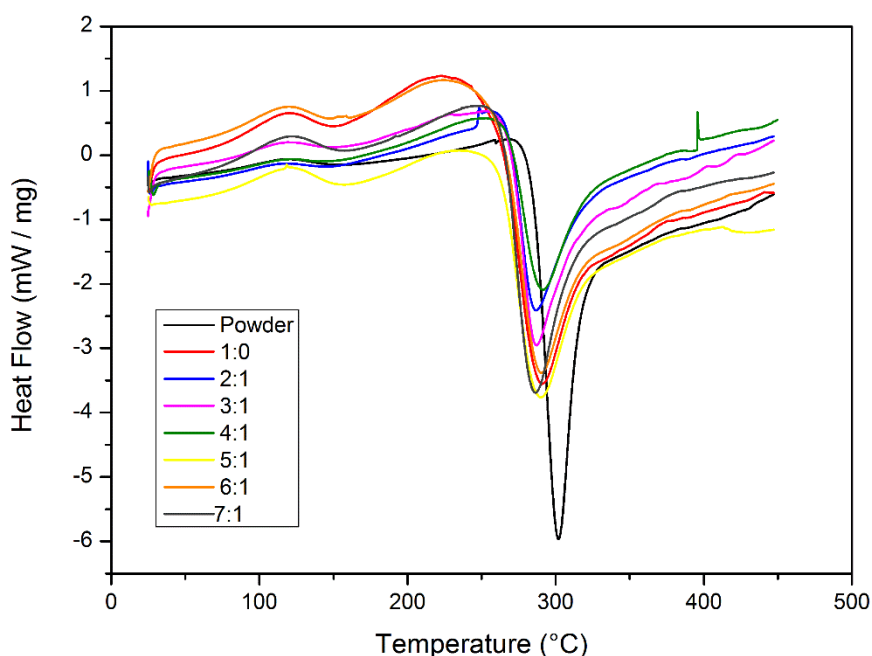
Similar to the present work, Rupiasih, Sumadiyasa e Putra (2017) did not notice significant differences in the chitosan content used in the membranes and their crystallinity index. Arantes *et al.* (2014) also associated drying as a crucial step in the nucleation and growth of crystallites. Results presented by Zhuang, Zhong e Zhao (2019) explained that chitosan chains with higher degrees of deacetylation are more compact structures and facilitate the formation of hydrogen bonds, which promotes an increase in the crystallinity of the films.

It is possible to notice two effects on the crystallinity index values presented in the work: first, a decrease in the initial value of the precursor powder sample, followed by a less pronounced drop in the optimal values of the solvent ratio. In this way, we can conclude that the first decrease is associated with the shaping of the membrane with its respective drying, and the second and lower decrease is associated with the effect of acetone.

4.4 THERMAL PROPERTIES

Figure 20 shows the thermograms of the membranes with 1.0 wt% chitosan according to the water:acetone volume ratio used. The thermograms were presented to demonstrate the thermal behavior of the membranes against a heating curve after a stage of thermal drying of the material. For simplification, it was tested in only one solid loading as a proof of concept of acetone influence in chitosan membrane thermal properties.

Figure 20- DSC thermograms of the powder and membranes containing 1 wt% chitosan with different water:acetone solvent ratio.



Ref: Author (2021).

In these thermograms, it is possible to identify the glass transition temperature (T_g) at the inflection point of each curves ($\sim 135^\circ\text{C}$), and the starting degradation temperature (T_{onset}) ($\sim 240^\circ\text{C}$) represented as the onset temperature of the exothermic peak, where the degradation of glucosamine units occurs (GUINESI; CAVALHEIRO, 2006). To facilitate understanding, Table 6 presents the mentioned values compared to the composition of the membranes and the degree of deacetylation shown in Figure 18.

Table 6- Glass transition temperature (T_g) and onset degradation temperature (T_{onset}) beginning of the chitosan powder and membranes containing 1 wt% with increasing acetone/water solvent ratio.

Sample	Water:Acetone	Degree of	T_g (°C)	T_{onset} (°C)
	Volume Ratio (v:v)	Deacetylation (%)		
1	Powder	76.56	136	273
2	1:0	94.24	136	244
3	2:1	88.01	131	260
4	3:1	91.32	135	255
5	4:1	97.39	134	253
6	5:1	53	136	244
7	6:1	94	136	246
8	7:1	98.48	137	251

Ref: Author (2021).

The literature comments that the temperature of thermal degradation of chitosan is a function of the degree of deacetylation and the crystallinity index of the material. Analyzing the isolated effect itself, amino radicals have lower thermal stability than acetamido radicals, which leads to a decrease in T_{onset} with the increase in DD. Otherwise, the CI, on the other hand, is directly proportional to the increase in T_{onset} , with a more significant effect than the DD (DELEZUK; PAVINATTO; CAMPANA FILHO, 2014; GUINESI; CAVALHEIRO, 2006).

Therefore, correlating the expressive drop in the CI presented in Table 5, the powder sample has superior thermal stability to all other synthesized membranes. Otherwise, according to the composition change of the membrane samples, there is an expected proportional increase of T_{onset} and DD until sample 5. However, in samples 6,7,8 it was not possible to correlate an effect of DD in T_{onset} , with this value tending to remain constant. Possibly some effect related to the properties of these membranes, such as porosity, for example.

Regarding T_g , practically no change in any of the samples was observed, neither in the powder sample nor in the membranes. This behavior was already expected since although there is a physical-chemical interaction in the membranes and concerning the amount of solvent, little change in T_g has been reported in the literature for different DD (DONG *et al.*, 2004).

4.5 MEMBRANE MICROSTRUCTURE

The N₂ adsorption and desorption isotherms (Figure 21) are presented to quantify and qualify the presence of pores in the reference membranes (without acetone) and their optimal porosity conditions for each solid content.

From the isotherms presented in Figure 21, some factors can be identified. First, all the samples possess mixtures of Type II and IV isotherms, which characterizes duplicity of pore size distribution in the meso and macroporous range (BARRET; JOYNER, 1951; SING, 2001). It is also noted the presence of capillary condensation, represented by the appearance of the same type of hysteresis in all samples, classified as Type H3, which characterizes slit-shaped pores (LOWELL *et al.*, 2004; SING; WILLIAMS, 2004).

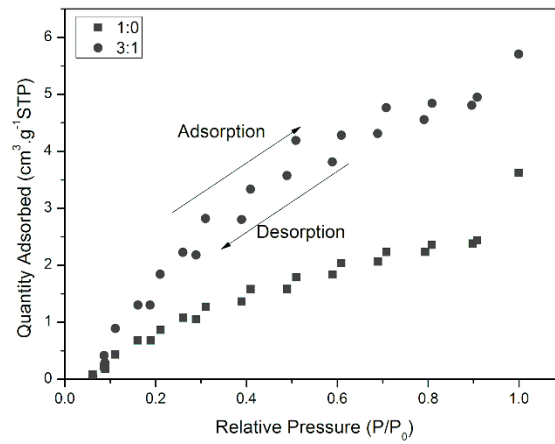
Regarding the variations in the membrane compositions, it is possible to notice a greater amount of gas adsorbed on the membranes in the optimized acetone additions, indicating an increase in porosity in the system as already reported in Figure 16. At the last point of relative pressure ($P/P_0 = 1$), a significant increase is observed when compared to the previous point, which is directly proportional to the solids content used, and indicates an expressive fraction of macropores in all membranes with a trend to increase in solids contents.

Figure 22 presents FEG-SEM surface pictures for membranes with some selected water:acetone volume ratios and chitosan amounts. It is possible to confirm the slit-like pore behavior with significant small pore size (<100 nm). The micrographs also shown there is no change in pore morphology between all membranes tested, the microstructure tends to have porous isotropy (same pore size in comparison to upper and lower membrane surface) and no pore large than 1 μm was found.

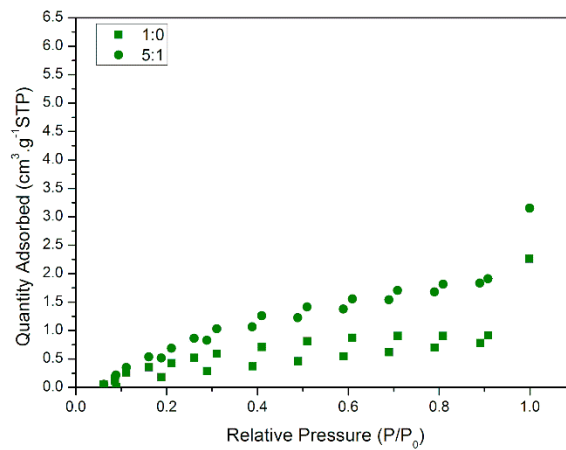
It is known from literature that non-rigid absorbent tends to promote a plate like particles morphology and consequently a pore in slit like form (THOMMES *et al.*, 2015). Several works in literature has obtained porous chitosan in the same pore morphology, even in different shaping routes (ALABDULJABBAR *et al.*, 2021; KUMAR; PILLAY; CHOONARA, 2021; LUO; BAI; ZHU, 2018).

Therefore, the pore formation mechanism in the chitosan membrane is linked to the chain mobility of the bulk system in the solvent during the slow drying procedure. For that reason, it is possible to notice at Figure 22 a higher presence of slit pores in lower solids contents, and this could explain the higher open porosity in Figure 16.

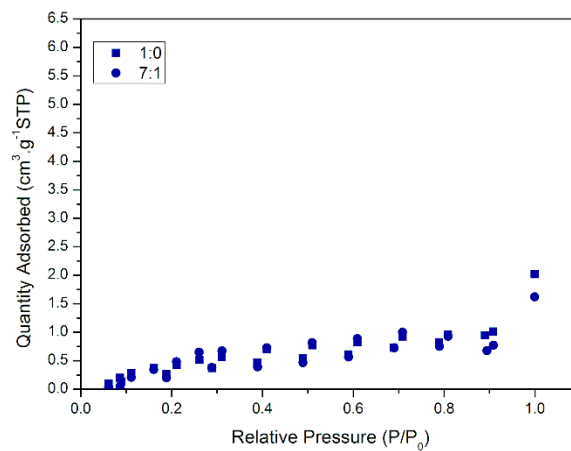
Figure 21- Nitrogen adsorption-desorption isotherms for membranes with some selected water:acetone volume ratios and chitosan: (a) 0.5 wt%, (b) 1.0 wt% and (c) 2.0 wt%.



(a)

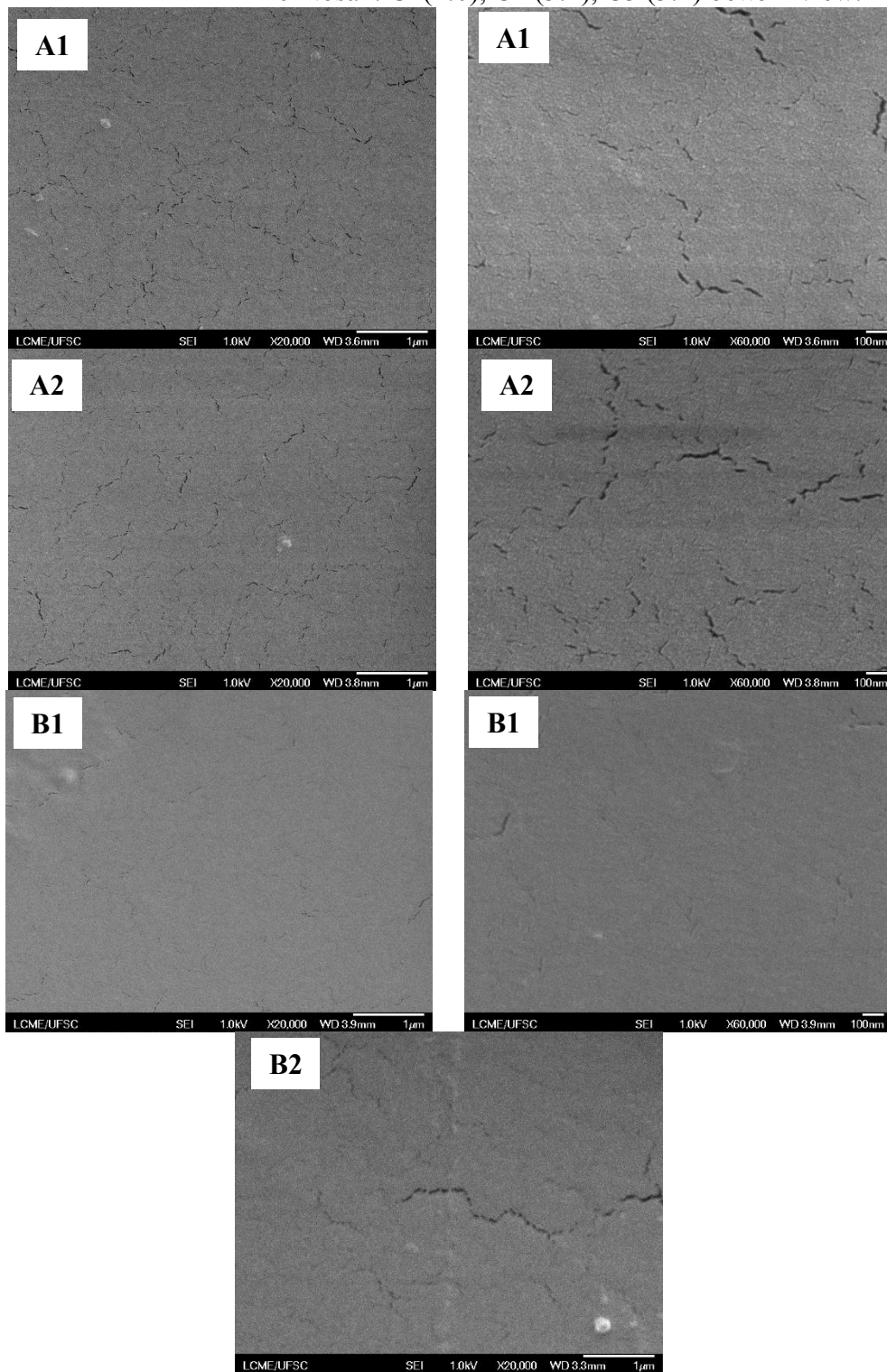


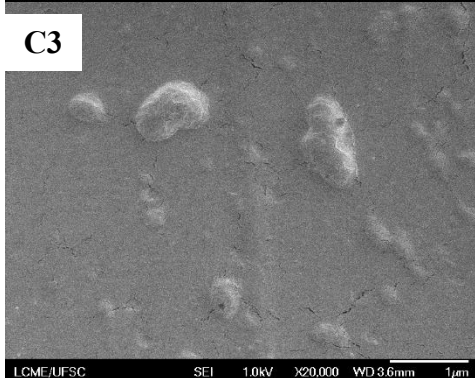
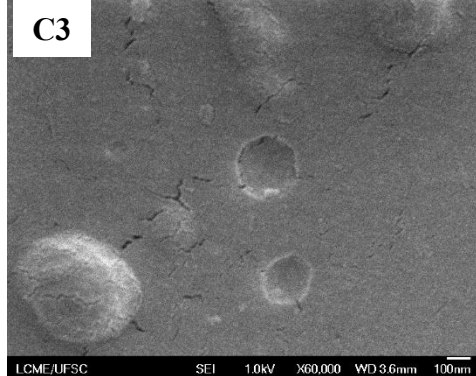
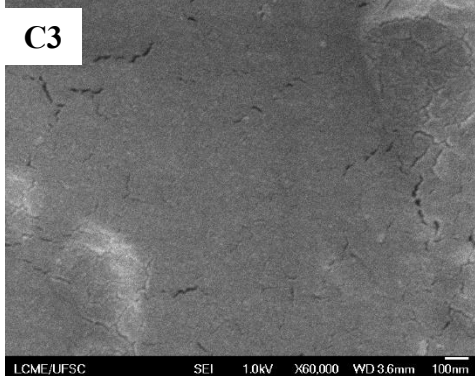
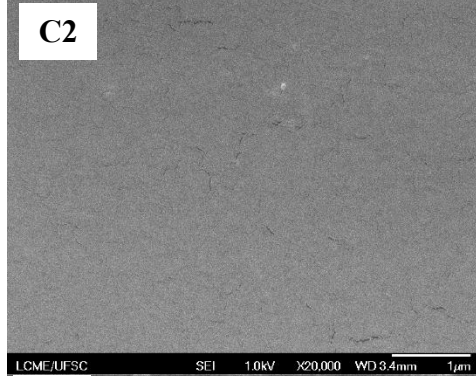
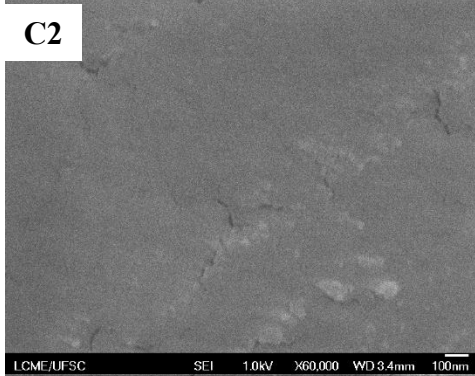
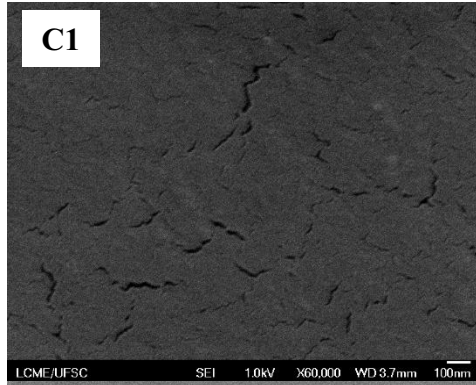
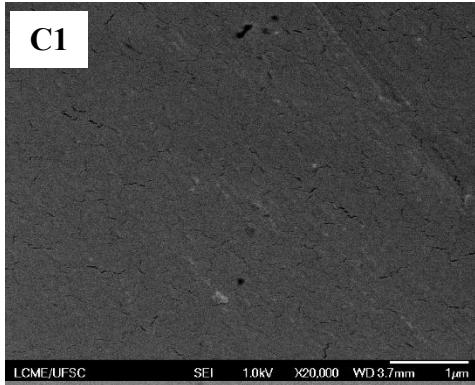
(b)



(c)

Figure 22- FEG-SEM pictures of the membranes with: (a) 1 wt% chitosan containing the following water/acetone ratio: A1 (1:0), A2 (5:1), (b) 2 wt% chitosan : B1 (1:0), B2 (7:1) (c) 0.5 wt% chitosan: C1(1:0), C2 (3:1), C3 (3:1) bottom view.





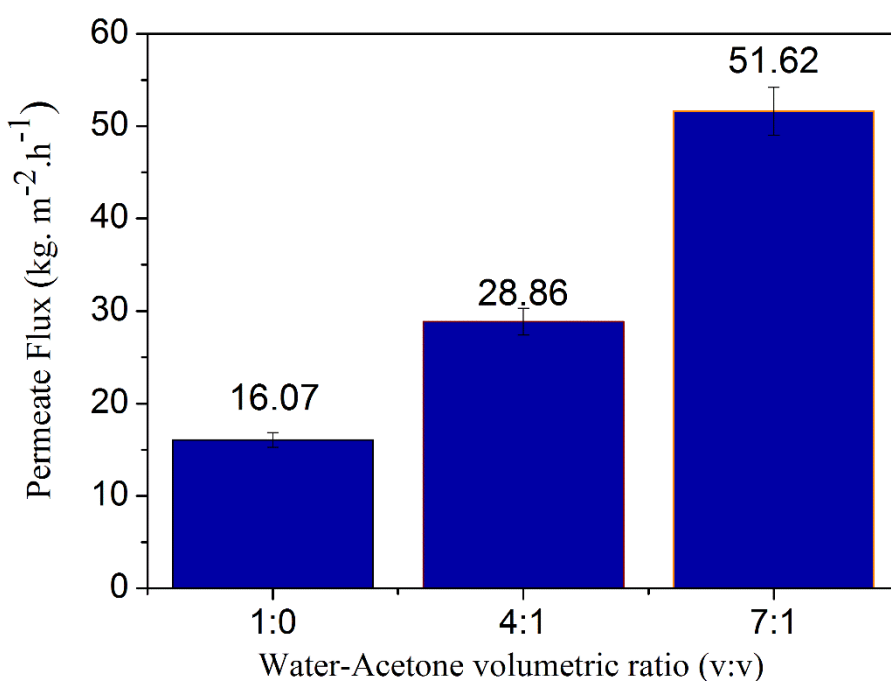
Ref: Author (2021).

4.6 PERFORMANCES OF MEMBRANES IN MD

The performance of porous chitosan membranes was evaluated in the DCMD unit. The tests showed an influence of chitosan concentration on the MD process and those only membranes prepared with 2 wt% chitosan exhibit permeate flux.

According to the membrane characterization, samples containing 0.5 and 1.0 wt% of chitosan are more hydrophilic based on the results of contact angle, swelling index, and open porosity, therefore these membranes are not proper to work in the membrane distillation process without a surface modification and a support layer addition. In this sense, the 1:0, 4:1, and 7:1 water/acetone membranes with 2 wt% chitosan were selected as exploratory test because it was necessary to evaluate the non-presence of acetone in direction to the higher porosity obtained in that solid loading, aiming to identify the membrane performance in three different open porosity values in chitosan membrane. The results of these tests are shown in Figure 23.

Figure 23- Pure water permeate flux with 2 wt% chitosan in the membrane distillation unit during 1 h.



Ref: Author (2022).

The water/acetone 7:1 membrane showed higher permeate flux, which can be attributed to its high porosity, its heterogeneous pore distribution, and its low degree of deacetylation, followed

by the 4:1 membrane. The lowest permeate flux value was obtained with the 1:0 membrane, without acetone. These results comprise the importance of proper optimization of solvents composition to achieve a better membrane performance. It is known from the literature that permeation flux in the membrane distillation process is strongly affected by the membrane material, surface characteristics, pore morphology, interconnectivity as well as membrane conformation process (ALKHUDHIRI; DARWISH; HILAL, 2012; EYKENS *et al.*, 2017).

Normally, commercial MD membranes, such as PVDF, PP, or PTFE possess a distilled water permeation flux at 1 h in the same operational conditions between $10 - 25 \text{ kg}\cdot\text{m}^{-2}\cdot\text{h}^{-1}$ (RAMLOW, 2018; RAMLOW *et al.*, 2019; SRISURICHAN; JIRARATANANON; FANE, 2006; TOLENTINO FILHO *et al.*, 2022). The higher flux obtained in the chitosan membranes (51.62 - 16.07) is very interesting for further application and could be explained by a synergistic combination of the chitosan properties allied to structure improvement provided by the acetone addition.

Previous work have demonstrated that the slit-like pores (Figure 22) exhibit high permeate flux with same porosity and transmembrane pressure than other pore morphology (HAN *et al.*, 2020), ascribed to the larger pore size and interconnected pore structure of the slit-like pore geometry (KANANI *et al.*, 2010).

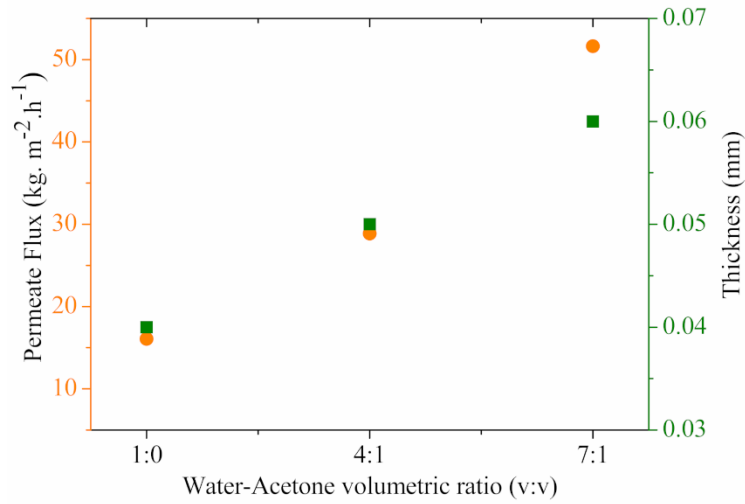
The effects of thickness, degree of deacetylation, and porosity in relation to permeate flux are shown in Figure 24. The thickness (Figure 24a) of the membrane has an important effect on mass transfer, normally decreasing membrane thickness would facilitate the transport mechanism and lead to an improved flux.

However, this could not be noticed in the chitosan membranes studied, due to the thickness variation that is low in comparison to other properties, such as open porosity, which were enhanced. In other way, the lower chitosan membrane thickness in comparison to the values in commercial MD membranes (EYKENS *et al.*, 2017) might explain some of this elevated flux obtained.

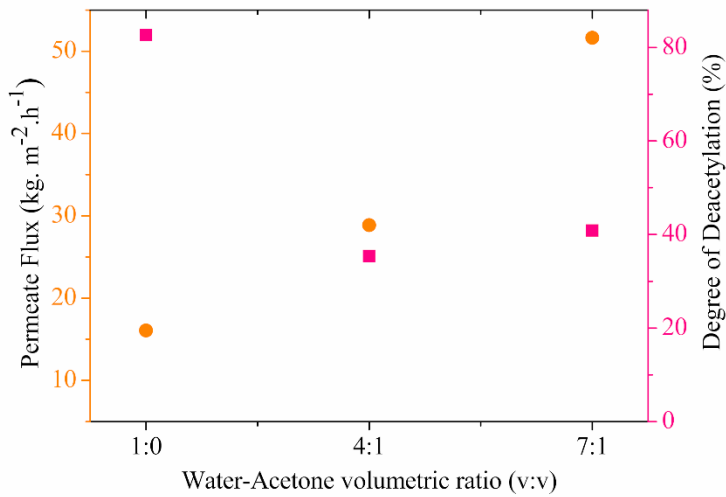
Figure 24b shows that the lower the degree of deacetylation, the greater the permeate flow. The increase in the degree of deacetylation is not thermodynamically favorable and can impair mass transfer and steam in the MD process due to the inherent hydrophilicity of the amino groups, which make the whole MD system more prone to wetting.

Generally, membranes with high porosity are very beneficial for membrane distillation, as this aspect can provide more pore passages for the diffusion of steam, leading to a high permeation flux. As seen in Figure 24c, the 1:0, 4:1, and 7:1 water/acetone membranes showed a directional proportion increase in both open porosity and permeate flux.

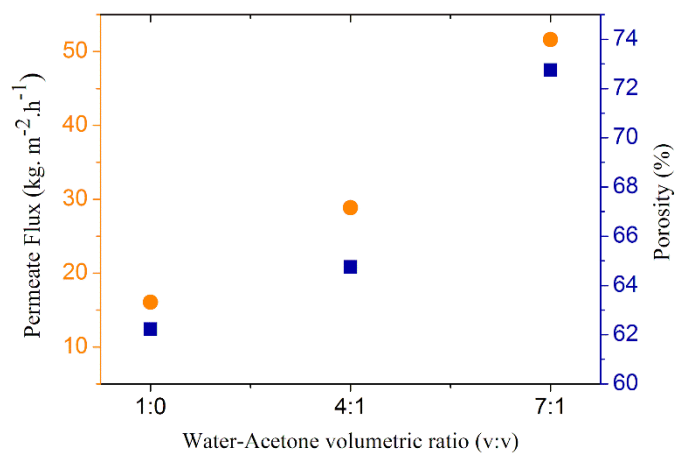
Figure 24- Effect of the thickness (a), degree of deacetylation (b) and porosity (c) in relation to pure water permeate flux test for membrane 2 wt% chitosan in a membrane distillation unit for 1h.



(a)



(b)



(c)

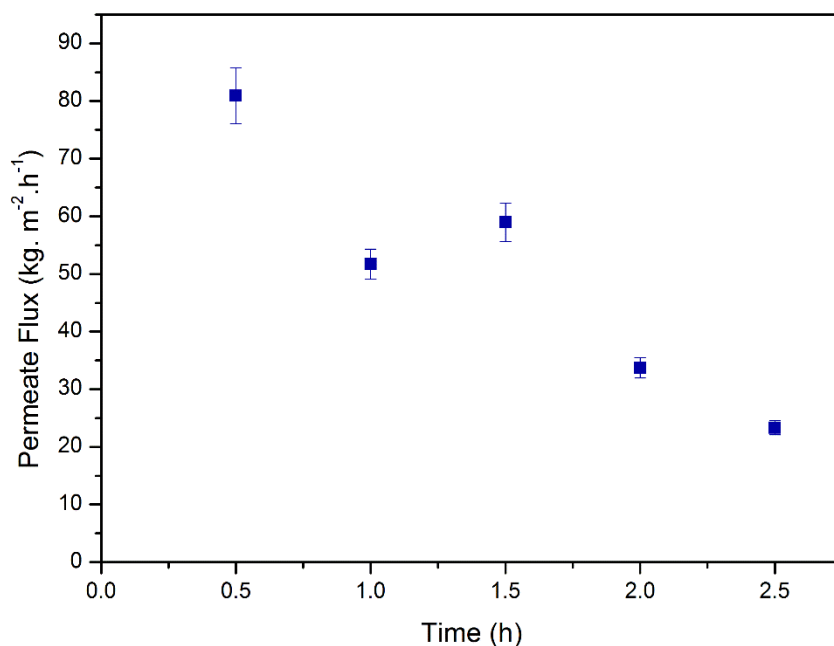
Ref: Author (2022).

Therefore, as explained in Figure 23, there is not one single effect that could change the membrane performance. The results obtained in characterization can provide multiple different effects on membrane performance and selectivity.

For example, the contact angle (Figure 14) of 4:1 membrane is higher than the 1:0 which can explain a improved permeability tendency, however although the 7:1 membrane possess a lower contact angle, almost equal as the 1:0 membrane, the elevated porosity combined with multimodal slit pore size structure produces an increase in system permeability.

Figure 25 displays the permeate flux for the chitosan membrane 2 wt% at 7:1 solvent/non-solvent volumetric ratio in the membrane distillation unit. It is possible to observe that the maximum value is reached in the first 30 min of application, followed by a decrease tendency in the subsequent times.

Figure 25- Water permeate flux test on different times for membrane 2 wt% chitosan at 7:1 water/acetone volume ratio in the membrane distillation unit.



Ref: Author (2022).

Although the high flux obtained, the MD process in the chitosan membrane was limited to a maximum of 2.5 h of application. After this period the membrane selected becomes very prone to

wetting, which makes unfeasible the correct MD process. The membrane properties that enables higher permeate flux are the adequate pore size and distribution, the high porosity, the hydrophobicity and the lower liquid degree absorption (SILVA *et al.*, 2021b).

Regarding membrane microstructure, chitosan starts with high liquid water resistance and a lower liquid absorption that provide an elevated permeate flux at beginning of membrane permeation process. However, as the process continues a mechanism of partial wetting occur making some partial pore blockage in contact with water vapor and significant decrease permeate flux in a short time period. At some moment, the flux decrease is so expressive that chitosan membrane is complete wetting, which make impossible a longer period of MD.

Aiming to improve this operation time of the process, processing parameters can be adjusted, such as feed temperature and flow, or the membrane material in which hydrophobicity also can be improved.

Liquid entry pressure (LEP) values are strongly associated with maximum pore size, porosity, and hydrophobicity of the membranes (ALKHUDHIRI; DARWISH; HILAL, 2012). Lower LEP values were obtained experimentally in the chitosan membrane rather than the values of commercial membranes (Table 8), corroborating the explanation in Figure 25 that the chitosan membranes obtained are more prone to wetting than PTFE or PVDF membranes. The chitosan membranes' LEP values were similar in comparison to PP membranes, mostly because of the higher pore size and porosity and lower contact angle of the commercial PP membranes. However, PP membranes can support longer operation periods experiments. Furthermore, as explained before in Figure 25, surface modifications could be performed to improve membrane hydrophobicity and the operational distillation conditions can be selected to provide improved conditions for chitosan membrane, such as lowering the feed flow or the system operating temperature.

Table 7- Comparison of experimental Liquid Entry Pressure (LEP) values in distilled water for PTFE, PP, PVDF commercial macroporous (pore size>50 nm) membranes, and chitosan membrane obtained.

Material	Open Porosity (%)	Experimental LEP (bar)	REFERENCES
PTFE	77	3.6	(SILVA <i>et al.</i> , 2021b)
PP	83	1.2	
PVDF	75	3.1	
Chitosan	72	1.1	This Work

Ref: Author (2022).

With all these results, it is possible to observe that the porous chitosan membranes tested in the process of membrane distillation with distilled water were successful until 2.5 h, providing high values of permeate flux, thus making these membranes good candidates to be tested in desalination and/or effluent treatment, although some improvements in processing conditions and membrane hydrophobicity could provide a higher LEP and stabilization flux for an enhanced membrane distillation process with chitosan membrane.

4.7 OVERVIEW

As an overview for the characterization results, Table A2 (APPENDIX) is presented to summarize the effects noticed in chitosan solid loading and acetone addition. The results emphasized the importance to properly define the solid amount to be adopted and the volumetric ratio of solvents applied.

Generally, a highly porous structure is produced from a thermodynamic compatible system. A non-rigid porous structure with slit-pore morphology is natural from the properties of chitosan material. Lower solid contents possess higher mobility and consequently an elevated porosity. In relation to the acetone concentration there is an optimal concentration value in porosity generation.

Up certain amount, acetone can improve polymer chain movement and increase system porosity, after that concentration there is a start of an effect tending to decrease system porosity and improve material hydrophobicity. More characterization studies are needed, such as mercury intrusion porosimetry to further determine the macroporous average pore size and distribution.

In the optimized condition, the membranes shows moderate hydrophobic wettability linked with high porosity, a lower degree of deacetylation, and a pore size and in meso and macroporous size range with slit-like pore shaping. All these conditions make the membrane developed here an interesting material to be applied in the membrane distillation process.

5 CONCLUSIONS AND OUTLOOK

5.1 CONCLUSIONS

Chitosan porous membrane synthesis by solvent evaporation technique employing acetone as non-solvent was successfully performed. First of all, the solubility of chitosan is limited by the solid loading and solvents' volume ratio. The synthesis route allowed to obtain membranes with high porosity, moderate hydrophobicity, and enhanced swelling index. Acetone was efficient as a porous agent and provide hydrophobicity in certain amount. Its volume ratio are related to the most desired results is strongly linked to chitosan concentration (3:1 in 0.5 wt%, 5:1 in 1.0 wt%, and 7:1 in 2.0 wt%).

According to the FTIR analysis, chemical reaction is associated with the presence of acetone in the membrane composition, making changes in an acetamido surface group absorbance, and in some cases, a nitrile bond is noticed. However, more studies must be carried out to propose a correct structure and reaction mechanism to understand the final chemical structure achieved.

The degree of deacetylation analysis indicates that the action of acetone against the functional groups of chitosan is a function of the chitosan concentration, and the water:acetone volume ratio. Moreover, the decrease in amino groups may be associated with increases in the contact angle present in samples with 1 and 2 wt% chitosan.

The crystallinity index value has changed from the initial powder sample, but no strong alterations are observed between membrane composition systems. T_g remains constant in all membranes tested, but T_{onset} tends to be affected in relation to acetone volume employed.

N_2 adsorption and desorption isotherms disclose that the membranes are in the meso and macroporous size range containing slit-like pores. The addition of optimal acetone concentration provides more heterogeneous pore size distribution. The sample porous surface morphology is confirmed by FEG-SEM, presenting small slit pore sizes with isotropy and interconnectivity.

The pure water permeation test in membrane distillation unit was successful for membranes containing 2 wt% chitosan. The permeate flux obtained with distilled water was quite expressive. Thus, chitosan membranes are promising candidates for an evaluation of real effluent membrane distillation separation. Nevertheless, some improvements in processing conditions and membrane hydrophobicity could provide a higher LEP and stabilization flux for enhanced membrane distillation.

5.2 OUTLOOK

For the continuation of this work, some suggestions are listed:

- a) Test the production of chitosan membrane in the presence of other types of materials and solvent:non-solvent components and some additives;
- b) Apply the obtained membrane in other membrane separation processes than MD;
- c) Improve the hydrophobicity of synthesized chitosan membrane for a better MD performance;
- d) Perform MD test in different kinds of effluents.

REFERENCES

- ABU-ZEID, M. A. E. R. *et al.* A comprehensive review of vacuum membrane distillation technique. **Desalination**, v. 356, p. 1–14, 2015.
- ADHAM, S. *et al.* Application of Membrane Distillation for desalting brines from thermal desalination plants. **Desalination**, v. 314, p. 101–108, 2013.
- AL-GHARABLI, S. *et al.* Biomimetic hybrid membranes with covalently anchored chitosan – Material design, transport and separation. **Desalination**, v. 491, p. 114550–114567, 2020.
- ALABDULJABBAR, F. A. *et al.* TiO₂ nanostructured coated functionally modified and composite electrospun chitosan nanofibers membrane for efficient photocatalytic degradation of organic pollutant in wastewater. **Journal of Materials Research and Technology**, v. 15, p. 5197–5212, nov. 2021.
- ALI, A. *et al.* On Designing of Membrane Thickness and Thermal Conductivity for Large Scale Membrane Distillation Modules. **Journal of Membrane Science & Research**, v. 2, p. 179–185, 2016.
- ALKHUDHIRI, A.; DARWISH, N.; HILAL, N. Membrane distillation: A comprehensive review. **Desalination**, v. 287, p. 2–18, 2012.
- ALZHRANI, S.; MOHAMMAD, A. W. Challenges and trends in membrane technology implementation for produced water treatment : A review. **Journal of Water Process Engineering**, v. 4, p. 107–133, 2014.
- ARANTES, M. K. *et al.* Influence of the drying route on the Depolymerization and properties of chitosan. **Polymer Engineering and Science**, p. 1–08, 2014.
- ARDESHIRI, F. *et al.* A hydrophilic-oleophobic chitosan/SiO₂ composite membrane to enhance oil fouling resistance in membrane distillation. **Korean Journal of Chemical Engineering**, v. 36, n. 2, p. 255–264, 2019.
- ASHOOR, B. B. *et al.* Principles and applications of direct contact membrane distillation (DCMD): A comprehensive review. **Desalination**, v. 398, p. 222–246, 2016.
- ASIF, M. B. *et al.* Acid mine drainage and sewage impacted groundwater treatment by membrane distillation: Organic micropollutant and metal removal and membrane fouling. **Journal of Environmental Management**, v. 291, p. 112708, ago. 2021.
- AYUNI, N. P. S.; YUNINGRAT, N. W. Study of Creatinine Transport through Chitosan/Pectin/Poly(Vinyl Alcohol) Blend Membranes. **Indonesian Journal of Biotechnology**, v. 21, n. 2, p. 102, 2017.
- BAKSHI, P. S. *et al.* Chitosan as an environment friendly biomaterial – a review on recent modifications and applications. **International Journal of Biological Macromolecules**, v. 150, p. 1072–1083, 2020.
- BARRET, E. P.; JOYNER, L. G. Determination of Nitrogen Adsorption-Desorption Isotherms. **Analytical Chemistry**, v. 23, n. 5, p. 79–80, 1951.
- BASKAR, D.; KUMAR, T. S. S. Effect of deacetylation time on the preparation, properties and

- swelling behavior of chitosan films. **Carbohydrate Polymers**, v. 78, n. 4, p. 767–772, 2009.
- BEPPU, M. M.; ARRUDA, E. J.; SANTANA, C. C. Síntese e caracterização de estruturas densas e porosas de quitosana. **Polímeros**, v. 9, n. 4, p. 163–169, 1999.
- BIRON, D. DA S.; SANTOS, V. DOS; ZENI, M. **Ceramic Membranes Applied in Separation Processes**. Caxias do Sul-RS, Rio Grande do Sul Brazil: Springer International Publishing AG, 2018.
- BONYADI, E. *et al.* A well-designed polystyrene/polycarbonate membrane for highly saline water desalination using DCMD process. **Desalination**, v. 528, p. 115604, abr. 2022.
- BORGOHAIN, R. *et al.* A review on chitosan-based membranes for sustainable CO₂ separation applications: Mechanism, issues, and the way forward. **Carbohydrate Polymers**, v. 267, p. 118178, 2021.
- BRACONNOT, H. Sur la nature des champignons. **Ann. Chim (Paris)**, v. 79, p. 265–304, 1811.
- CADOGAN, E. I. *et al.* Characterization, fouling, and performance of synthesized chitosan–glycerol membranes in bacterial removal from municipal wastewater. **Desalination and Water Treatment**, v. 57, n. 38, p. 17670–17682, 2016.
- CAMACHO, L. M. *et al.* Advances in membrane distillation for water desalination and purification applications. **Water (Switzerland)**, v. 5, n. 1, p. 94–196, 2013.
- CAMPOS, M. G. N. *et al.* Chitosan cross-linked films for drug delivery application. **Macromolecular Symposia**, v. 279, n. 1, p. 169–174, 2009.
- CASTRO-MUÑOZ, R. *et al.* Towards azeotropic MeOH-MTBE separation using pervaporation chitosan-based deep eutectic solvent membranes. **Separation and Purification Technology**, v. 281, p. 119979, 2022.
- CASTRO-MUÑOZ, R.; GONZÁLEZ-VALDEZ, J.; AHMAD, M. Z. High-performance pervaporation chitosan-based membranes : new insights and perspectives. **Reviews in Chemical Engineering**, v. 37, n. 8, p. 959–974, 2021.
- CHEN, P. H. *et al.* Improvement in the properties of chitosan membranes using natural organic acid solutions as solvents for chitosan dissolution. **Journal of Medical and Biological Engineering**, v. 27, n. 1, p. 23–28, 2007.
- CHUANG, Y. J.; CHEN, M. J.; CHEN, P. R. Fabrication and permeability characteristics of microdialysis probe using chitosan nanoporous membrane. **Journal of Nanomaterials**, v. 2014, 2014.
- CHUNG, H. W. *et al.* Multistage vacuum membrane distillation (MSVMD) systems for high salinity applications. **Journal of Membrane Science**, v. 497, p. 128–141, 2016.
- CRINI, G. *et al.* Metal removal from aqueous media by polymer-assisted ultrafiltration with chitosan. **Arabian Journal of Chemistry**, v. 10, p. S3826–S3839, 2017.
- CRISCUOLI, A.; BAFARO, P.; DRIOLI, E. Vacuum membrane distillation for purifying waters containing arsenic. **Desalination**, v. 323, p. 17–21, 2013.
- CUI, Z.; BEACH, E. S.; ANASTAS, P. T. Modification of chitosan films with environmentally benign reagents for increased water resistance. **Green Chemistry Letters and Reviews**, v. 4, n. 1,

p. 35–40, 2011.

DELEZUK, J. A. DE M.; PAVINATTO, A.; CAMPANA FILHO, S. P. Effects of Chitosan Characteristics on Its Thermal Stability. **Brazilian Journal of Thermal Analysis**, v. 3, n. 3–4, p. 36, 2014.

DELGADO-RANGEL, L. H. *et al.* Deep eutectic solvent-assisted phase separation in chitosan solutions for the production of 3D monoliths and films with tailored porosities. **International Journal of Biological Macromolecules**, v. 164, p. 4084–4094, 2020.

DOMSZY, J.; ROBERTS, G. Evaluation of infrared spectroscopic techniques for analysing chitosan. **Die Makromolekulare Chemie**, v. 186, n. 8, p. 1671–1677, 1985.

DONG, Y. *et al.* Studies on glass transition temperature of chitosan with four techniques. **Journal of Applied Polymer Science**, v. 93, n. 4, p. 1553–1558, 2004.

DUONG, H. C. *et al.* Membrane Distillation for Seawater Desalination Applications in Vietnam: Potential and Challenges. **Vietnam Journal of Science and Technology**, v. 55, n. 6, p. 659, 2017.

ESMAEILI, M.; RAJABI, L.; BAKHTIARI, O. Preparation and characterization of chitosan-boehmite nanocomposite membranes for pervaporative ethanol dehydration. **Journal of Macromolecular Science, Part A: Pure and Applied Chemistry**, v. 56, n. 11, p. 1022–1034, 2019.

EYKENS, L. *et al.* Influence of membrane thickness and process conditions on direct contact membrane distillation at different salinities. **Journal of Membrane Science**, v. 498, p. 353–364, 2016a.

EYKENS, L. *et al.* How to select a membrane distillation configuration? Process conditions and membrane influence unraveled. **Desalination**, v. 399, p. 105–115, 2016b.

EYKENS, L. *et al.* Membrane synthesis for membrane distillation: A review. **Separation and Purification Technology**, v. 182, p. 36–51, 2017.

FORTUNATO, L. *et al.* Textile dye wastewater treatment by direct contact membrane distillation: Membrane performance and detailed fouling analysis. **Journal of Membrane Science**, v. 636, p. 119552, 2021.

GONG, D. *et al.* Interfacial Ions Sieving for Ultrafast and Complete Desalination through 2D Nanochannel Defined Graphene Composite Membranes. **ACS Nano**, v. 15, n. 6, p. 9871–9881, 2021.

GONZÁLEZ, D.; AMIGO, J.; SUÁREZ, F. Membrane distillation: Perspectives for sustainable and improved desalination. **Renewable and Sustainable Energy Reviews**, v. 80, p. 238–259, 2017.

GOOSEN, M. E. A. **Applications of chitin and chitosan**. Lancaster: Technomic Publishing Company, 1996.

GRYTA, M. The study of performance of polyethylene chlorinetrifluoroethylene membranes used for brine desalination by membrane distillation. **Desalination**, v. 398, p. 52–63, 2016.

GRZYBEK, P. *et al.* Robust and high selective chitosan asymmetric Membranes: Relation between microporous structure and pervaporative efficiency in ethanol dehydration. **Separation and Purification Technology**, v. 281, p. 119897, 2022.

GUINESI, L. S.; CAVALHEIRO, É. T. G. The use of DSC curves to determine the acetylation degree of chitin/chitosan samples. **Thermochimica Acta**, v. 444, n. 2, p. 128–133, 2006.

GUO, J. *et al.* Elucidating the fouling mechanism in pharmaceutical wastewater treatment by membrane distillation. **Desalination**, v. 475, p. 114148, 2020.

GUPTA, N.; KUSHWAHA, A. K.; CHATTOPADHYAYA, M. C. Adsorptive removal of Pb 2+, Co 2+ and Ni 2+ by hydroxyapatite/chitosan composite from aqueous solution. **Journal of the Taiwan Institute of Chemical Engineers**, v. 43, n. 1, p. 125–131, 2012.

HAN, C. *et al.* Improved performance of thin-film composite membrane supported by aligned nanofibers substrate with slit-shape pores for forward osmosis. **Journal of Membrane Science**, v. 612, p. 118447, 2020.

HONG, H.; WEI, J.; LIU, C. Development of asymmetric gradational-changed porous chitosan membrane for guided periodontal tissue regeneration. **Composites Part B: Engineering**, v. 38, n. 3, p. 311–316, 2007.

HOPPE-SEYLER, F. Ueberchitin und cellulose. **Ber. Deut. Chem. Ges.**, v. 27, p. 3329–3331, 1894.

JAIN, A. *et al.* A new horizon in modifications of chitosan: Syntheses and applications. **Critical Reviews in Therapeutic Drug Carrier Systems**, v. 30, n. 2, p. 91–181, 2013.

KALLA, S. Use of membrane distillation for oily wastewater treatment - A review. **Journal of Environmental Chemical Engineering**, v. 9, n. 1, 2021.

KAMIŃSKI, WŁ.; MODRZEJEWSKA, Z. Application of Chitosan Membranes in Separation of Heavy Metal Ions. **Separation Science and Technology**, v. 32, n. 16, p. 2659–2668, 1997.

KANANI, D. M. *et al.* Permeability–selectivity analysis for ultrafiltration: Effect of pore geometry. **Journal of Membrane Science**, v. 349, n. 1–2, p. 405–410, 2010.

KEZIA, K. *et al.* Direct contact membrane distillation for the concentration of saline dairy effluent. **Water Research**, v. 81, p. 167–177, 2015.

KHRAISHEH, M.; ALMOMANI, F.; AL-GHOUTI, M. Electrospun Al₂O₃ hydrophobic functionalized membranes for heavy metal recovery using direct contact membrane distillation. **International Journal of Energy Research**, v. 45, n. 6, p. 8151–8167, 2021.

KIM, C. H. *et al.* Improvement of the Biocompatibility of Chitosan Dermal Scaffold by Rigorous Dry Heat Treatment. **Macromolecular Research**, v. 12, n. 4, p. 367–373, 2004.

KIM, H. C. *et al.* Membrane distillation combined with an anaerobic moving bed biofilm reactor for treating municipal wastewater. **Water Research**, v. 71, p. 97–106, 2015.

KIM, K. M. *et al.* Properties of Chitosan Films as a Function of pH and Solvent type. **Journal of Food Science**, v. 71, n. 3, p. 119–124, 2006.

KIM, S. *et al.* Development of chitosan-ellagic acid films as a local drug delivery system to induce apoptotic death of human melanoma cells. **Journal of Biomedical Materials Research - Part B Applied Biomaterials**, v. 90 B, n. 1, p. 145–155, 2009.

KIM, S.; LEE, D. W.; CHO, J. Application of direct contact membrane distillation process to treat anaerobic digestate. **Journal of Membrane Science**, v. 511, p. 20–28, 2016.

- KUMAR, P.; PILLAY, V.; CHOONARA, Y. E. Macroporous chitosan/methoxypoly(ethylene glycol) based cryosponges with unique morphology for tissue engineering applications. **Scientific Reports**, v. 11, n. 1, p. 3104, 2021.
- KUMAR, R. V. *et al.* Advanced oxidation technologies combined with direct contact membrane distillation for treatment of secondary municipal wastewater. **Process Safety and Environmental Protection**, v. 140, p. 111–123, 2020.
- LI, K. **Ceramic Membranes for Separation and Reaction**. London- UK: John Wiley & Sons, Ltd, 2007.
- LLANOS, J. H. R.; VERCİK, L. C. DE O.; VERCİK, A. Physical Properties of Chitosan Films Obtained after Neutralization of Polycation by Slow Drip Method. **Journal of Biomaterials and Nanobiotechnology**, v. 06, n. 04, p. 276–291, 2015.
- LOWELL, S. *et al.* **Characterization of Porous Solids and Powders Surface Area, Pore Size and Density**. Springer Science+Business Media, LLC, Originally published by Kluwer Academic Publishers, 2004.
- LUO, W.; BAI, Z.; ZHU, Y. Fast removal of Co(II) from aqueous solution using porous carboxymethyl chitosan beads and its adsorption mechanism. **RSC Advances**, v. 8, n. 24, p. 13370–13387, 2018.
- MADALOSSO, H. *et al.* Modeling and experimental validation of direct contact membrane distillation applied to synthetic dye solutions. **Journal of Chemical Technology & Biotechnology**, v. 96, n. 4, p. 909–922, out. 2020.
- MADALOSSO, H. B. *et al.* Membrane Surface Modification by Electrospinning, Coating, and Plasma for Membrane Distillation Applications: A State-of-the-Art Review. **Advanced Engineering Materials**, v. 2001456, p. 1–26, 2021.
- MADALOSSO, H. B. **Modification of commercial polymeric membranes via electrospraying for membrane distillation applications aiming to water recovery from textile wastewater**. 2021.- Dissertação de Mestrado, Departamento de Engenharia Química e Alimentos, Universidade Federal de Santa Catarina, Florianópolis/Santa Catarina, 2021.
- MANNA, A. K.; PAL, P. Solar-driven flash vaporization membrane distillation for arsenic removal from groundwater: Experimental investigation and analysis of performance parameters. **Chemical Engineering and Processing: Process Intensification**, v. 99, p. 51–57, 2016.
- MARQUES, J. S. *et al.* Removal of aqueous copper(II) by using crosslinked chitosan films. **Reactive and Functional Polymers**, v. 134, p. 31–39, 2019.
- MARTÍNEZ-CAMACHO, A. P. *et al.* Chitosan composite films: Thermal, structural, mechanical and antifungal properties. **Carbohydrate Polymers**, v. 82, n. 2, p. 305–315, 2010.
- MOKHTAR, N. M. *et al.* Preparation and characterization of PVDF membranes incorporated with different additives for dyeing solution treatment using membrane distillation. **Desalination and Water Treatment**, v. 56, n. 8, p. 1999–2012, 2015.
- MOZIA, S. *et al.* Evaluation of performance of hybrid photolysis-DCMD and photocatalysis-DCMD systems utilizing UV-C radiation for removal of diclofenac sodium salt from water. **Polish Journal of Chemical Technology**, v. 15, n. 1, p. 51–60, 2013.

- MULDER, M. **Basic Principles of Membrane Technology**. Amsterdam- Netherlands: Kluwer Academic Publishers, 1996.
- MURALI, V. P. *et al.* Modified electrospun chitosan membranes for controlled release of simvastatin. **International Journal of Pharmaceutics**, v. 584, n. May, p. 119438, 2020.
- NASROLLAHZADEH, M. *et al.* Starch, cellulose, pectin, gum, alginate, chitin and chitosan derived (nano)materials for sustainable water treatment: A review. **Carbohydrate Polymers**, v. 251, n. May 2020, p. 116986, 2021.
- OSÓRIO, L. R. *et al.* Antibacterial activity of a chitosan derivative obtained in the absence of a solvent. **Materials Science Forum**, v. 869, p. 869–873, 2016.
- PAKDEL, P. M.; PEIGHAMBARDOUST, S. J. Review on recent progress in chitosan-based hydrogels for wastewater treatment application. **Carbohydrate Polymers**, v. 201, p. 264–279, 2018.
- PEARCE, G. Introduction to membranes: Filtration for water and wastewater treatment. **Filtration & Separation**, v. 44, n. 2, p. 24–27, 2007.
- PENDERGAST, M. M.; HOEK, E. M. V. A review of water treatment membrane nanotechnologies. **Energy & Environmental Science**, v. 4, p. 1946–1971, 2011.
- PHATTARANAWIK, J.; JIRARATANANON, R.; FANE, A. G. Effect of pore size distribution and air flux on mass transport in direct contact membrane distillation. **Journal of Membrane Science**, v. 215, n. 1–2, p. 75–85, 2003.
- PICKER-FREYER, K.; BRINK, D. Evaluation of powder and tableting properties of chitosan. **American Association of Pharmaceutical Scientist Technology Journal**, v. 7, n. 3, p. 1-10, 2006
- PRIYADARSHI, R.; RHIM, J. W. Chitosan-based biodegradable functional films for food packaging applications. **Innovative Food Science and Emerging Technologies**, v. 62, n. 102346, p. 1–20, 2020.
- QASIM, A. *et al.* A perspective on dual purpose gas hydrate and corrosion inhibitors for flow assurance. **Journal of Petroleum Science and Engineering**, v. 183, n. December 2018, p. 106418, 2019.
- QUIST-JENSEN, C. A. *et al.* A study of membrane distillation and crystallization for lithium recovery from high-concentrated aqueous solutions. **Journal of Membrane Science**, v. 505, p. 167–173, 2016a.
- QUIST-JENSEN, C. A. *et al.* Direct contact membrane distillation for the concentration of clarified orange juice. **Journal of Food Engineering**, v. 187, p. 37–43, 2016b.
- RADHAKUMARY, C. *et al.* HEMA-grafted chitosan for dialysis membrane applications. **Journal of Applied Polymer Science**, v. 101, n. 5, p. 2960–2966, 2006.
- RAMLOW, H. **Destilação por membrana aplicada ao tratamento de águas residuais da indústria têxtil**. 2018.- Dissertação de Mestrado, Departamento de Engenharia Química e Alimentos, Universidade Federal de Santa Catarina, Florianópolis/Santa Catarina, 2018.
- RAMLOW, H. *et al.* Direct Contact Membrane Distillation Applied to Colored Reactive or Disperse Dye Solutions. **Chemical Engineering and Technology**, v. 42, n. 5, p. 1045–1052, 2019.

RAMLOW, H.; MACHADO, R. A. F.; MARANGONI, C. Direct contact membrane distillation for textile wastewater treatment: A state of the art review. **Water Science and Technology**, v. 76, n. 10, p. 2565–2579, 2017.

RAMYA, R. *et al.* Biomedical applications of chitosan: An overview. **Journal of Biomaterials and Tissue Engineering**, v. 2, n. 2, p. 100–111, 2012.

RASHID, S. *et al.* Preparation and properties of chitosan–metal complex: Some factors influencing the adsorption capacity for dyes in aqueous solution. **Journal of Environmental Sciences**, v. 66, p. 301–309, 2018.

REZAEI, M. *et al.* **Wetting phenomena in membrane distillation: Mechanisms, reversal, and prevention**. Elsevier B.V., 2018. v. 139

RIAZ RAJOKA, M. S. *et al.* Chitosan and its derivatives: synthesis, biotechnological applications, and future challenges. **Applied Microbiology and Biotechnology**, v. 103, n. 4, p. 1557–1571, 2019.

RIZEQ, B. R. *et al.* Synthesis , Bioapplications , and Toxicity Evaluation of Chitosan-Based Nanoparticles. **International Journal of Molecular Science**, v. 20, p. 1–24, 2019.

ROBERTS, G. A. F. **Chitin Chemistry**. Sereal Untuk. 1992.

RODRIGUES, C. **NANOCOMPÓSITOS DE QUITOSANA-ARGILA-ZnO**. 2018.- Dissertação de Mestrado, Departamento de Engenharia Química e Alimentos, Universidade Federal de Santa Catarina, Florianópolis/Santa Catarina, 2018.

ROUGET, C. Des substances amylacees dans les tissus des animaux, specialement des Articules (chitine). **Comp. Rend.**, v. 48, p. 792–795, 1859.

ROY, J. C. *et al.* Solubility of Chitin: Solvents, Solution Behaviors and Their Related Mechanisms. In: **Solubility of Polysaccharides**. p. 109–129, 2017.

RUPIASIH, N. N. *et al.* Utilization of Shrimp Skin Waste (Sea Lobster) As Raw Material for the Membrane Filtration. **Journal of Physics: Conference Series**, v. 846, n. 1, 2017.

RUPIASIH, N. N.; SUMADIYASA, M.; PUTRA, I. K. The Effect of Variations in the Ratio of Matrix/Solvent on the Physical and Mechanical Properties of Chitosan Biopolymer Membranes. **IOP Conference Series: Materials Science and Engineering**, v. 196, n. 1, 2017.

SAHEBJAMEE, N. *et al.* Preparation and characterization of porous chitosan–based membrane with enhanced copper ion adsorption performance. **Reactive and Functional Polymers**, v. 154, n. June, p. 104681, 2020.

SAHRANAVARD, M. *et al.* A critical review on three dimensional-printed chitosan hydrogels for development of tissue engineering. **Bioprinting**, v. 17, n. e00063, p. 1–9, 2020.

SAID, I. A. *et al.* Sweeping gas membrane distillation (SGMD) for wastewater treatment, concentration, and desalination: A comprehensive review. **Chemical Engineering and Processing - Process Intensification**, v. 153, p. 107960–107971, 2020.

SAMPATH, U. G. T. M. *et al.* Fabrication of porous materials from natural/synthetic biopolymers and their composites. **Materials**, v. 9, n. 12, p. 1–32, 2016.

SANTOS, B. DE C. **Configurações multitéstágio de destilação por membrana de contato direto**

para recuperação de água residual de tingimento têxtil. 2021.- Dissertação de Mestrado, Departamento de Engenharia Química e Alimentos, Universidade Federal de Santa Catarina, Florianópolis/Santa Catarina, 2021.

SEDELKIN, V. M. *et al.* Preparation and Characterization of Chitosan Pressure-Driven Filtration Membranes. **Membranes and Membrane Technologies**, v. 1, n. 5, p. 306–315, 2019.

SHAHU, V. T.; THOMBRE, S. B. Air gap membrane distillation: A review. **Journal of Renewable and Sustainable Energy**, v. 11, n. 4, 2019.

SHARIATINIA, Z. Pharmaceutical applications of chitosan. **Advances in Colloid and Interface Science**, v. 263, p. 131–194, 2019.

SILVA, A. O. *et al.* Chitosan as a matrix of nanocomposites: A review on nanostructures, processes, properties, and applications. **Carbohydrate Polymers**, v. 272, n. July, p. 118472, 2021a.

SILVA, R. DE S. *et al.* Membrane Distillation: Experimental evaluation of Liquid Entry Pressure in commercial membranes with textile dye solutions. **Journal of Water Process Engineering**, v. 44, n. July, p. 102339, 2021b.

SILVA, R. DE S. *et al.* Understanding the effects of operational conditions on the membrane distillation process applied to the recovery of water from textile effluents. **Process Safety and Environmental Protection**, v. 145, p. 285–292, 2021c.

SILVA, R. S. *et al.* Steady state evaluation with different operating times in the direct contact membrane distillation process applied to water recovery from dyeing wastewater. **Separation and Purification Technology**, v. 230, n. August 2019, p. 115892, 2020.

SILVESTRE, W. P.; BALDASSO, C.; TESSARO, I. C. Potential of chitosan-based membranes for the separation of essential oil components by target-organophilic pervaporation. **Carbohydrate Polymers**, v. 247, p. 116676–116687, 2020.

SING, K. The use of nitrogen adsorption for the characterisation of porous materials. **Colloids and Surfaces A: Physicochemical and Engineering Aspects**, v. 187–188, p. 3–9, 2001.

SING, K. S. W.; WILLIAMS, R. T. Physisorption hysteresis loops and the characterization of nanoporous materials. **Adsorption Science and Technology**, v. 22, n. 10, p. 773–782, 2004.

SONG, W. *et al.* Functionalized superhydrophobic biomimetic chitosan-based films. **Carbohydrate Polymers**, v. 81, n. 1, p. 140–144, 2010.

SRISURICHAN, S.; JIRARATANANON, R.; FANE, A. G. Mass transfer mechanisms and transport resistances in direct contact membrane distillation process. **Journal of Membrane Science**, v. 277, n. 1–2, p. 186–194, 2006.

SULTANA, N. *et al.* Chitosan-based nanocomposite scaffolds for tissue engineering applications. **Materials and Manufacturing Processes**, v. 30, n. 3, p. 273–278, 2015.

THIRUGNANASAMBANDHAM, K.; SIVAKUMAR, V.; MARAN, J. P. Application of chitosan as an adsorbent to treat rice mill wastewater—Mechanism, modelling and optimization. **Carbohydrate Polymers**, v. 97, n. 2, p. 451–457, 2013.

THOMMES, M. *et al.* Physisorption of gases, with special reference to the evaluation of surface area and pore size distribution (IUPAC Technical Report). **Pure and Applied Chemistry**, v. 87, n.

9–10, p. 1051–1069, 2015.

TLILI, I. *et al.* Flat sheet direct contact membrane distillation study to decrease the energy demand for solar desalination purposes. **Sustainable Energy Technologies and Assessments**, v. 52, p. 102100, 2022.

TOLENTINO FILHO, C. M. *et al.* Influence of multi-component composition of dyeing bath in the membrane distillation performance. **Process Safety and Environmental Protection**, v. 156, p. 184–195, 2021.

TOLENTINO FILHO, C. M. *et al.* Membrane distillation for the recovery textile wastewater: Influence of dye concentration. **Journal of Water Process Engineering**, v. 46, p. 102611–102620, 2022.

TOMASZEWSKA, M.; BIAŁOŃCZYK, L. Ethanol production from whey in a bioreactor coupled with direct contact membrane distillation. **Catalysis Today**, v. 268, p. 156–163, 2016.

UMOREN, S. A.; EDUOK, U. M. Application of carbohydrate polymers as corrosion inhibitors for metal substrates in different media: A review. **Carbohydrate Polymers**, v. 140, p. 314–341, 2016.

VATANPOUR, V. *et al.* Polysaccharides in fabrication of membranes: A review. **Carbohydrate Polymers**, v. 281, p. 119041–119066, 2022.

VUNAIN, E.; MISHRA, A. K.; MAMBA, B. B. Dendrimers, mesoporous silicas and chitosan-based nanosorbents for the removal of heavy-metal ions: A review. **International Journal of Biological Macromolecules**, v. 86, p. 570–586, 2016.

WAN, Y. *et al.* Synthesis, characterization and ionic conductive properties of phosphorylated chitosan membranes. **Macromolecular Chemistry and Physics**, v. 204, n. 5–6, p. 850–858, 2003.

WANG, P.; CHUNG, T. S. Recent advances in membrane distillation processes: Membrane development, configuration design and application exploring. **Journal of Membrane Science**, v. 474, p. 39–56, 2015.

WANG, X. *et al.* Preparation and properties of chitosan/ poly(vinyl alcohol) blend foams for copper adsorption. **Polymer International**, v. 55, p. 1230–1235, 2006.

WOODS, J.; PELLEGRINO, J.; BURCH, J. Generalized guidance for considering pore-size distribution in membrane distillation. **Journal of Membrane Science**, v.368, p. 124-133, 2011.

WU, C. *et al.* Enhanced functional properties of biopolymer film incorporated with curcumin-loaded mesoporous silica nanoparticles for food packaging. **Food Chemistry**, v. 288, p. 139–145, 2019.

WU, Y. *et al.* Crystallization of calcium carbonate on chitosan substrates in the presence of regenerated silk fibroin. **Langmuir**, v. 27, n. 6, p. 2804–2810, 2011.

WU, Y. *et al.* Performance and fouling mechanism of direct contact membrane distillation (DCMD) treating fermentation wastewater with high organic concentrations. **Journal of Environmental Sciences**, v. 65, p. 253–261, 2018.

XU, D.; HEIN, S.; WANG, K. Chitosan membrane in separation applications. **Materials Science and Technology**, v. 24, n. 9, p. 1076–1087, 2008.

YANG, T.; ZALL, R. R. Chitosan Membranes for Reverse Osmosis Application. **Journal of Food**

Science, v. 49, n. 1, p. 91–93, 1984.

YE, Y. *et al.* Microbubble aeration enhances performance of vacuum membrane distillation desalination by alleviating membrane scaling. **Water Research**, v. 149, p. 588–595, 2019.

ZARGAR, V.; ASGHARI, M.; AFSARI, M. Gas separation properties of swelled nanocomposite chitosan membranes cross-linked by 3-aminopropyltriethoxysilane. **International Journal of Environmental Science and Technology**, v. 16, n. 1, p. 37–46, 2019.

ZAWADZKI, J.; KACZMAREK, H. Thermal treatment of chitosan in various conditions. **Carbohydrate Polymers**, v. 80, n. 2, p. 394–400, 2010.

ZENG, X.; RUCKENSTEIN, E. Control of pore sizes in macroporous chitosan and chitin membranes. **Industrial and Engineering Chemistry Research**, v. 35, n. 11, p. 4169–4175, 1996.

ZHANG, H.; ZHONG, Z.; XING, W. Application of ceramic membranes in the treatment of oilfield-produced water: Effects of polyacrylamide and inorganic salts. **Desalination**, v. 309, p. 84–90, 2013.

ZHAO, Q. S. *et al.* Preparation and characteristics of novel porous hydrogel films based on chitosan and glycerophosphate. **Carbohydrate Polymers**, v. 76, n. 3, p. 410–416, 2009.

ZHU, F. *et al.* A critical review on the electrospun nanofibrous membranes for the adsorption of heavy metals in water treatment. **Journal of Hazardous Materials**, v. 401, p. 1–22, 2021.

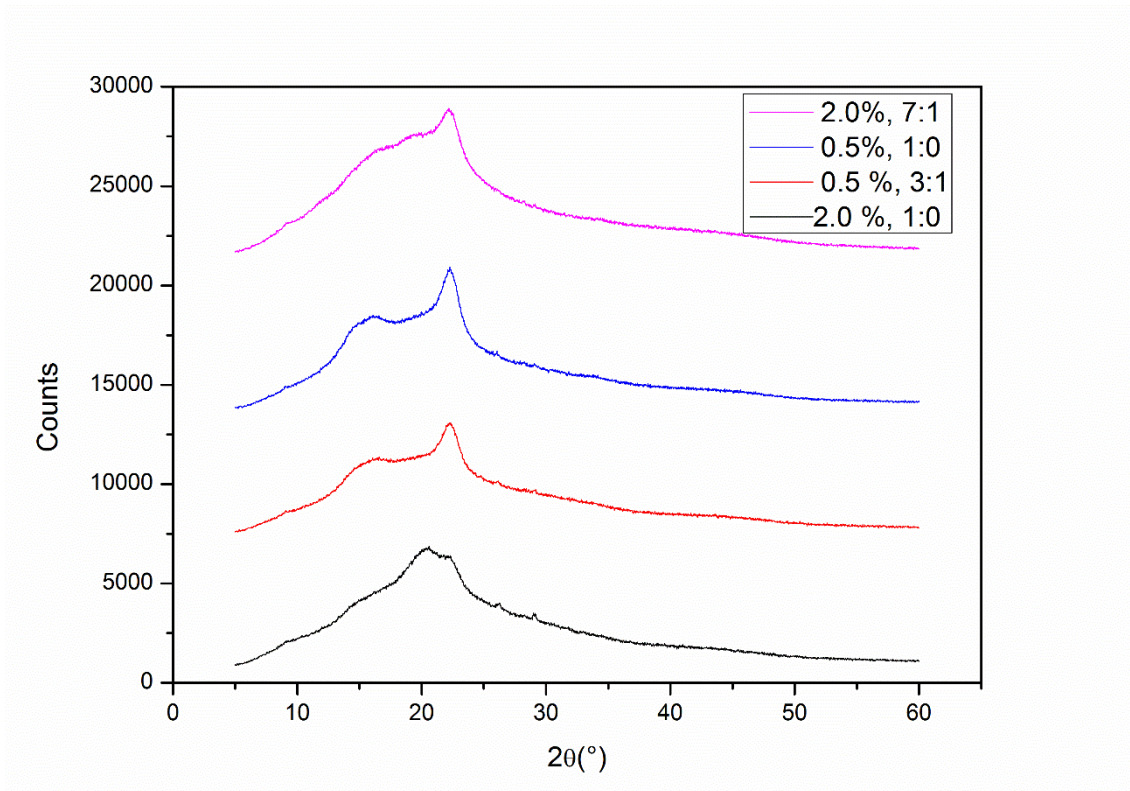
ZHU, J.; ARSOVSKA, B.; KOZOVSKA, K. A review: naturally available sources of chitosan and analysis of chitosan derivatives for its antimicrobial activity. **International Journal of Recent Scientific Research**, v. 8, n. 03, p. 15773–15776, 2017.

ZHUANG, C.; ZHONG, Y.; ZHAO, Y. Effect of deacetylation degree on properties of Chitosan films using electrostatic spraying technique. **Food Control**, v. 97, p. 25–31, 2019.

ZOLOTAREV, P. P. *et al.* Treatment of waste water for removing heavy metals by membrane distillation. **Journal of Hazardous Materials**, v. 37, p. 77–82, 1994.

APPENDIX A1- MEMBRANE CHARACTERIZATION

Figure A1: XRD spectrum for the for chitosan membrane containing 0.5 and 2.0 wt% without acetone and in the optimized water/acetone solvent ratio.



Ref: Author (2022).

APPENDIX A2- OVERVIEW OF THE MEMBRANE CHARACTERIZATION RESULTS

Table A2. Overview of the main characterization results on chitosan membranes.

Sample	Chitosan (wt%)	Water: Aceton (volume ratio)	Contact Angle (°)	Degree of Swelling (%)	Open Porosity (%)	Degree of Deacetylation (%)	Crystallinity Degree (%)
1	0.5	(1:0)	83.44 ± 1.24	405.04 ± 13.96	84.57 ± 1.78	94.31	0.3
2		(1:1)	90.48 ± 0.42	441.45 ± 82.23	86.19 ± 2.67	92.43	n.m.
3		(2:1)	86.57 ± 0.62	606.37 ± 94.04	90.20 ± 1.66	98.53	n.m.
4		(3:1)	83.53 ± 2.24	753.1 ± 38.9	92.08 ± 0.4	87.84	0.28
5		(4:1)	84.37 ± 1.31	459.65 ± 106.43	84.02 ± 3.23	94.21	n.m.
6		(5:1)	87.16 ± 0.16	429.97 ± 25.09	85.73 ± 0.8	n.m.	n.m.
7		(6:1)	83.13 ± 1.24	367.55 ± 97.38	82.66 ± 6.09	87.94	n.m.
8	1.0	(1:0)	86.19 ± 0.41	143.53 ± 24.17	67.36 ± 5.53	94.2	0.3
9		(2:1)	89.16 ± 3.46	163.02 ± 12.71	70.84 ± 1.88	88.01	0.31
10		(3:1)	99.34 ± 1.33	173.7 ± 40.21	70.88 ± 5.57	91.32	0.26
11		(4:1)	91.51 ± 2.37	247.11 ± 25.23	78.48 ± 2.19	97.39	0.30
12		(5:1)	88.17 ± 1.16	300.48 ± 19.53	81.77 ± 1.17	53	0.26
13		(6:1)	93.66 ± 0.64	237.65 ± 13.33	78.04 ± 1.22	94	0.29
14		(7:1)	100.01 ± 2.00	181.4 ± 17.69	72.88 ± 2.36	98.48	n.m
15		(8:1)	91.76 ± 0.58	164.99 ± 5.03	67.19 ± 4.97	n.m.	n.m
16	2.0	(1:0)	89.35 ± 0.58	108.81 ± 6.1	62.39 ± 1.73	82.7	0.3
17		(3:1)	98.333 ± 0.61	117.12 ± 1.65	63.74 ± 0.33	23.7	n.m.
18		(4:1)	102.14 ± 1.04	122.39 ± 3.62	64.75 ± 0.88	35.41	n.m.
19		(5:1)	112.133 ± 1.48	153.52 ± 25.29	68.88 ± 5.4	80.844	n.m.
20		(6:1)	102.5 ± 0.39	165.97 ± 6.46	71.39 ± 0.99	66	n.m.
21		(7:1)	91.37 ± 0.35	179.91 ± 17.65	72.75 ± 2.88	40.86	0.24
22		(8:1)	90.47 ± 0.3	131.45 ± 14.3	66.00 ± 3.45	44.53	n.m
23		(9:1)	89.57 ± 0.48	134.62 ± 2.2	66.89 ± 0.45	46.39	n.m.

Ref: Author (2021).